Lawrence Berkeley National Laboratory
Recent Work

Title
ELASTICALLY SCATTERED POLARIZATION OF 40-MeV PROTONS FROM DEUTERIUM

Permalink
https://escholarship.org/uc/item/7039w6sg

Author
Goldberg, Howard S.

Publication Date
1964-08-05

University of California

Ernest O. Lawrence Radiation Laboratory

ELASTICALLY SCATTERED POLARIZATION OF 40-MeV

PROTONS FROM DEUTERIUM

Berkeley, California

DISCLAIMER

UNIVERSITY OF CALIFORNIA

ELASTICALLY SCATTERED POLARIZATION OF 40-MeV PROTONS FROM DEUTERIUM

Howard S. Goldberg
(Ph. D. Thesis)

August 5, 1964

ELASTICALLY SCATTERED POLARIZATION OF 40-MeV PROTONS FROM DEUTERIUM

Contents

ELASTICALLY SCATTERED POLARIZATION OF 40-MeV PROTONS FROM DEUTERIUM

Howard S. Goldberg

Lawrence Radiation Laboratory
University of California
Berkeley, California

August 5, 1964

ABSTRACT

The polarization of the elastically scattered protons from deuterium at 40 MeV has been measured and found to be large, reaching a maximum negative value of -0.392 ± 0.018 at $\theta_{c.m.}$ = 114 deg and crossing over to positive values at backward c.m. angles. Our results do not agree with the impulse-approximation predictions of Kowalski and Feldman. After development of the density-matrix formalism for a spin 1/2, spin 1 system, a phase-shift analysis of the data was made, using the elastic differential cross section results of Williams. To get a reasonably good fit to the data, F waves had to be included. This required a 26-parameter fit, and for 62 data points gave a minimum χ^2 of 135. The large values of the mixing parameters in certain J states indicate the presence of tensor forces.

I. INTRODUCTION

In a recent paper, Kowalski and Feldman[1] have made an impulse-approximation (IA) calculation of the polarization induced in p-d scattering at 150, 90, and 40 MeV, taking into account the internal motion of the target nucleons and off-the-energy-shell scattering. The experiment presented here was undertaken, at 40 MeV, to make a direct comparison with their predictions. Also, it was hoped that the determination of the polarization in nucleon-deuteron scattering would provide information useful to the understanding of the large difference in polarization induced in nucleon-nucleon[2] scattering and that induced as a result of the scattering of a nucleon from a few-nucleon system.[3]

Since the Kowalski and Feldman predictions were not in agreement with our results, a different approach to the problem was attempted. The most direct method and one capable of utilizing the 40-MeV elastic differential cross section data of Williams[4] was a phase-shift analysis of the p-d system. An approach similar to that of Wolfenstein[5] and Stapp[6] was taken, using the density-matrix formalism, now for a spin (1/2, 1) system. Attempts at a (1/2, 1) analysis had been formalized by Budianskii[7] and Hsueh-tan[8] with conflicting results. Therefore, the phase-shift problem was carefully formalized along with a phase-shift analysis of the 40-MeV p-d scattering.

II. GENERAL CONSIDERATIONS

If one takes N_+ as the number of particles in a beam with their spins up and N_- as the number of particles with their spins down, then the polarization is defined as

$$P = \frac{N_+ - N_-}{N_+ + N_-},$$

so that an unpolarized beam can be considered to be an equal mixture of two completely and oppositely polarized beams, while a partially polarized beam would contain a fraction $|P|$ of a completely polarized beam and a fraction $1 - |P|$ of an unpolarized beam. [5]

If one tries an experiment and scatters an unpolarized beam off an unpolarized target and measures the left counts (L) at θ_L and the right counts (R) at $\theta_R = -\theta_L$, then the resulting asymmetry $\epsilon(\theta)$, defined as

$$\epsilon(\theta) = \frac{L(\theta_L) - R(\theta_R)}{L(\theta_L) + R(\theta_R)},$$

is zero. In other words, for the elastic differential cross section we have the well-known $\sigma_0(\theta) = \sigma_0(-\theta)$. However, if the incoming beam is polarized, then $\epsilon(\theta)$ is no longer necessarily found equal to zero, i.e.,

$$\sigma(\theta) \neq \sigma(-\theta) .$$

Now, if one were to scatter an unpolarized beam from an unpolarized target and take the resulting left-scattered beam (L) and scatter it off a second target, one would most likely find $\sigma_2(\theta) \neq \sigma_2(-\theta)$. Thus, from the discussion of the above paragraph, the resultant left-scattered beam from the first target must have been polarized. The first target, T_1, was capable of inducing a polarization at some angle θ and some energy E of the incoming beam, and this polarization was reflected in the second scattering, at T_2, which gave a nonzero asymmetry. This

polarization is characterized by a number $P_1(\theta)$, where 1 represents the kind of target T_1, and θ the scattering angle. The polarization has a direction $\hat{n}_1$, so that

$$\vec{P}_1(\theta) = P_1(\theta)\,\hat{n}_1 \ ,$$

where $\hat{n}_1 = \hat{k}_{in} \times \hat{k}_{out}$, $\hat{k}_{in}$ is a unit vector in the incident beam direction and $\hat{k}_{out}$ is a unit vector in the scattered beam direction. According to the Basle convention, positive polarization is taken along $\hat{n}$.

Finally, for a double scattering experiment, the elastic differential cross section for the second scattering is[5]

$$\sigma_p(\theta) = \sigma_0(\theta)\,(1 + P_1 P_2(\theta)\,\hat{n}_1 \cdot \hat{n}_2) \ .$$

This will be proved in a later section.

If one confines oneself to scattering in a plane perpendicular to the direction of $\hat{n}_1$, one will have

$$\epsilon(\theta) = \frac{\sigma_p(\theta_L) - \sigma_p(\theta_R)}{\sigma_p(\theta_L) + \sigma_p(\theta_R)} = \frac{L - R}{L + R}$$

$$= P_1 P_2(\theta) \ .$$

Therefore, by scattering polarized protons of polarization P_1 off a deuterium target and measuring $\epsilon(\theta)$ one can find, from $P_2(\theta) = \epsilon(\theta)/P_1$, the polarization that would have been induced by an unpolarized proton beam.
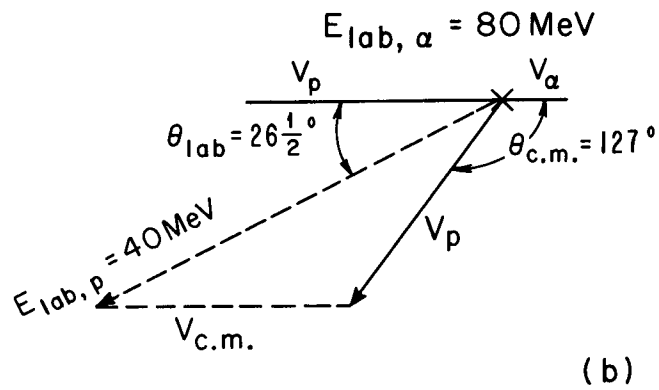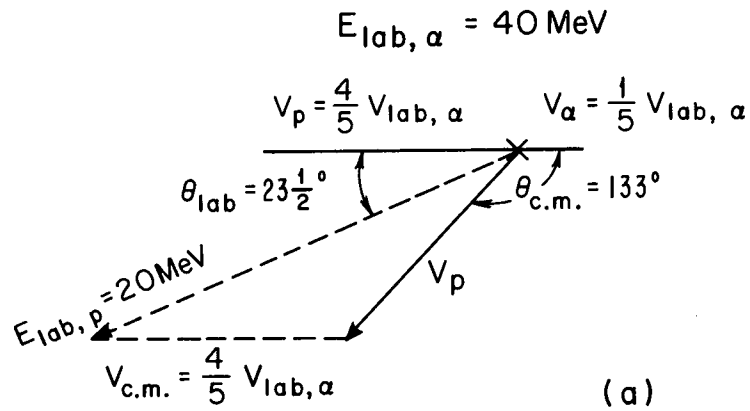
III. 40-MeV POLARIZED PROTON BEAM

The first step, then, in the experiment was to determine the polarization of the 40-MeV proton beam, which in effect necessitated a separate experiment. In order to clarify what follows a simple non-relativistic relation should be kept in mind:

$$E_{c.m.} = \frac{M}{m+M} E_L ,$$

where $E_{c.m.}$ is the total center-of-mass energy, E_L is the lab energy of the incoming particle of mass m, and M is the mass of the stationary target particle. Thus, if we have an α beam impinging on a hydrogen target, $E_{c.m.} = 1/5\ E_L$, while a proton beam impinging on a helium target would have $E_{c.m.} = 4/5\ E_L$, so that for the same center-of-mass energy for each system $E_{L,\alpha} = 4\ E_{L,p}$, i. e. , a 10-MeV proton beam striking a helium target would have the same c. m. energy as a 40-MeV α beam striking a hydrogen target.

The starting point of the polarization analysis for the 40-MeV proton beam was experimental data for the polarization of 10-MeV protons on helium.[9] With respect to the incoming proton direction, the maximum polarization occurs at $\theta_{c.m.}^{max} = 133$ deg, with a value of 99%. Using the results of the above discussion, one sees that the 10-MeV p-He scattering would have the same center-of-mass energy as a 40-MeV α-p scattering. The kinematical relations along with the c. m. and lab angles at $\theta_{c.m.}^{max}$ are shown in Fig. 1. Here v_α, v_p are the c. m. velocities of the alphas (incident in the lab) and the protons (lab target particles) respectively. Thus, with respect to the alpha beam direction, the maximum polarization occurs at $\theta_L^{max} = 23.5$ deg. By scattering a 40-MeV α beam off a liquid-nitrogen-cooled gaseous hydrogen target, we produced, at $\theta_L^{max} = 23.5$ deg, a 20-MeV proton beam polarized to 99%.

This beam was then scattered from a helium target, T_2, and the left-right asymmetry, $\epsilon(\theta) = (L - R)/(L + R)$, of the elastically scattered

$$E_{lab, \alpha} = 40 \, MeV$$

$$V_p = \frac{4}{5} V_{lab, \alpha} \qquad V_\alpha = \frac{1}{5} V_{lab, \alpha}$$

$$\theta_{lab} = 23\frac{1}{2}^\circ \qquad \theta_{c.m.} = 133^\circ$$

$$E_{lab, p} = 20 \, MeV$$

$$V_p$$

$$V_{c.m.} = \frac{4}{5} V_{lab, \alpha}$$

(a)

$$E_{lab, \alpha} = 80 \, MeV$$

$$V_p \qquad V_\alpha$$

$$\theta_{lab} = 26\frac{1}{2}^\circ \qquad \theta_{c.m.} = 127^\circ$$

$$E_{lab, p} = 40 \, MeV$$

$$V_p$$

$$V_{c.m.}$$

(b)

MU-34250

Fig. 1. The nonrelativistic vectoral relations between the c. m. velocities, v_α, v_p, and $v_{c.m.}$, showing the $\theta_{c.m.}$ at or close to the maximum polarization, along with the corresponding lab angle and recoil proton lab energy.

protons was measured. Since $\epsilon(\theta) = P_1 P(\theta)$, where P_1 is the polarization of the proton beam and $P(\theta)$ the proton polarization induced by scattering unpolarized protons from T_2, one can determine where the maximum value of the polarization occurs, from $\epsilon(\theta) = 0.99 \, P(\theta)$. The results are given in Table I and plotted in Fig. 2. The experimental apparatus was the same as that used in the p-d experiment, and is described in the following sections. From Fig. 2 one can see that for 20-MeV p-He elastic scattering the maximum polarization occurs at $\theta_{c.m.}^{max} = 126$ deg, with a value of +0.828 ± 0.02. The sign is given in accord with the Basle convention (positive polarization in the direction of $\vec{k}_{in} \times \vec{k}_{out}$). Because of a hurried first analysis of the data θ_L was taken, in the subsequent experiment, to be 127 deg, corresponding to a lab angle of 26.5 deg. Figure 1 shows this kinematically. Repeating the above procedure, we started with an 80-MeV α beam and extracted at $\theta_L = 26.5$ deg, a proton beam of 41.1 ± 0.6 MeV at the center of the hydrogen target, with a polarization of +0.819 ± 0.02. The intensity was 4×10^7 protons/sec for 10 μA of incident α-beam.

Table I. Proton polarization in p-He^4 elastic scattering at 20 MeV.

θ_L	$\theta_{c.m.}$	$P(\theta)$
25	31.2	-0.132 ± 0.005
35	43.5	-0.199 ± 0.005
57	69.5	-0.393 ± 0.005
62	74.8	-0.452 ± 0.006
70	83.6	-0.534 ± 0.007
76	90.0	-0.611 ± 0.007
81	95.5	-0.610 ± 0.014
87	101.9	-0.489 ± 0.018
92	106.8	-0.223 ± 0.024
100	114.5	$+0.420 \pm 0.042$
103	117.5	$+0.579 \pm 0.042$
106	120.0	$+0.780 \pm 0.028$
109	129.9	$+0.818 \pm 0.020$
112	125.8	$+0.828 \pm 0.020$
116	129.7	$+0.811 \pm 0.020$
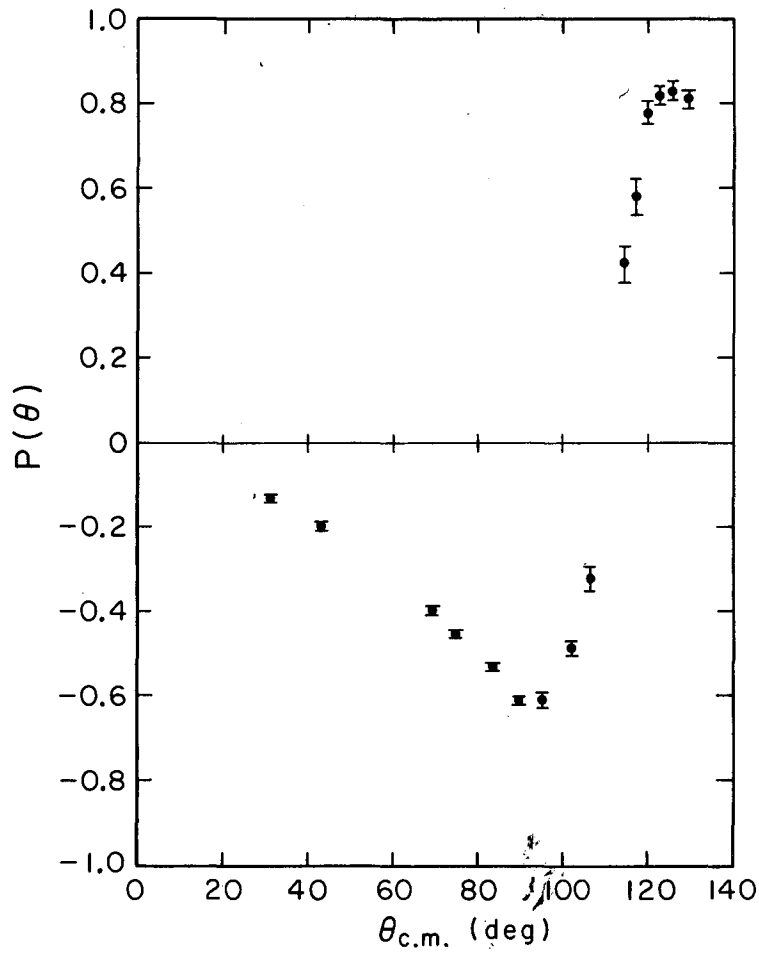
Fig. 2. Proton polarization in p-He^4 elastic scattering at 20 MeV.
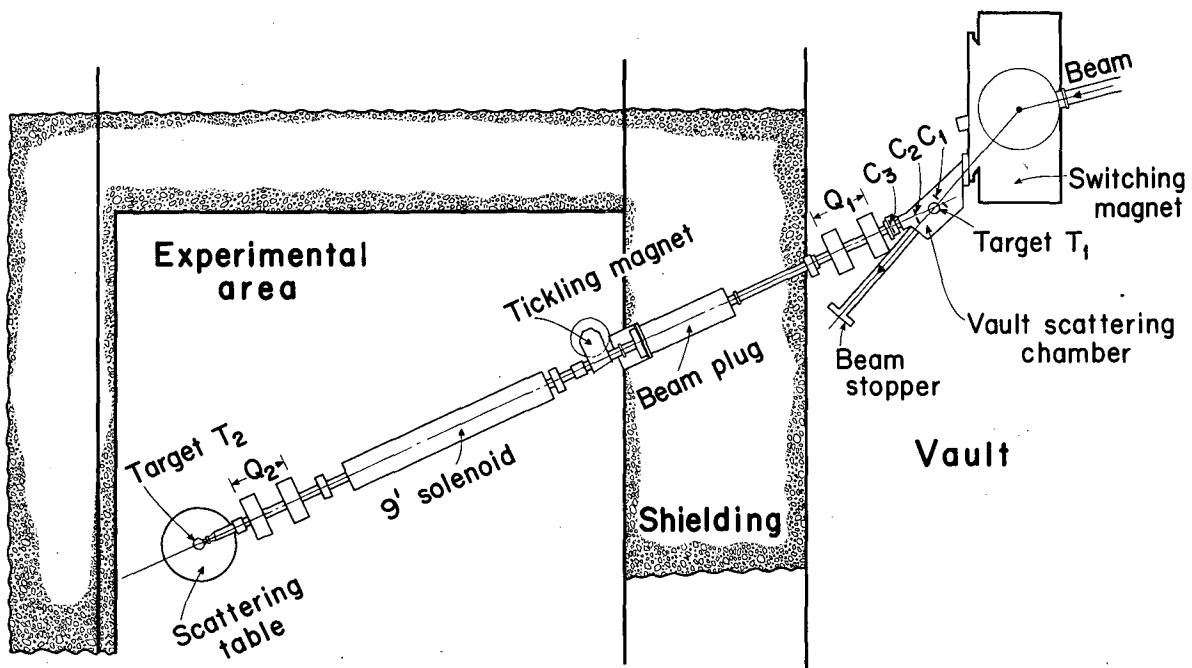
MU-34251

IV. EXPERIMENTAL SYSTEM

A. Beam Layout

The beam layout is shown in Fig. 3. After being steered by the switching magnet, the α beam entered the vault scattering chamber, where it was collimated (C_1) prior to hitting the vault target, T_1. The current of each half of C_1 was measured and balanced by using the switching magnet and the 88-in. quadrupoles (not shown) to keep the beam centered on the target. Target T_1 was a liquid-nitrogen-cooled gaseous hydrogen target, described elsewhere.[10] The target was run at 114 psia. The α energy was 84.5 MeV, which was reduced to 80 MeV at the target center by loss in the hydrogen gas and in the target entrance window.

The recoil polarized protons were taken off at the previously described angle (26.5 deg) and collimated by C_2 and C_3. The first collimator, C_2, was made of 0.100-in. tantalum with a $3/8 \times 3.5$-in. slot which defined the target width. The second collimator, C_3, was also 0.100-in. tantalum with a 1.5×3.5-in. slot which defined the solid angle. The second collimator defined the scattering angle to ± 1 deg. With a distance of 30 in. between the two collimators the penumbra region was negligible. The first quadrupole position was determined by the space limitations in the vault. The polarities were, in the horizontal plane, diverging (D) - converging (C) and C-D for quadrupoles 1 and 2, respectively, and the beam was rendered parallel between them. A ray trace for a central ray is shown in Fig. 4. OPTIK, an IBM-7090 program, was used to determine the quadrupole currents where their effective lengths and positions were used as input data. During the run the currents were juggled to optimize the proton beam current and minimize the beam spot size.

Shown in Fig. 3, but not used in the experiment, were a 9-ft solenoid and a tickling magnet. Eventually, the solenoid will be used to flip the spin of the polarized proton beam and the tickling magnet will be used to center the flipped beam.

Fig. 3. Plan view of experimental arrangement.

Vertical plane

C_2 C_3 Q_1

Shielding

Q_2

Horizontal plane
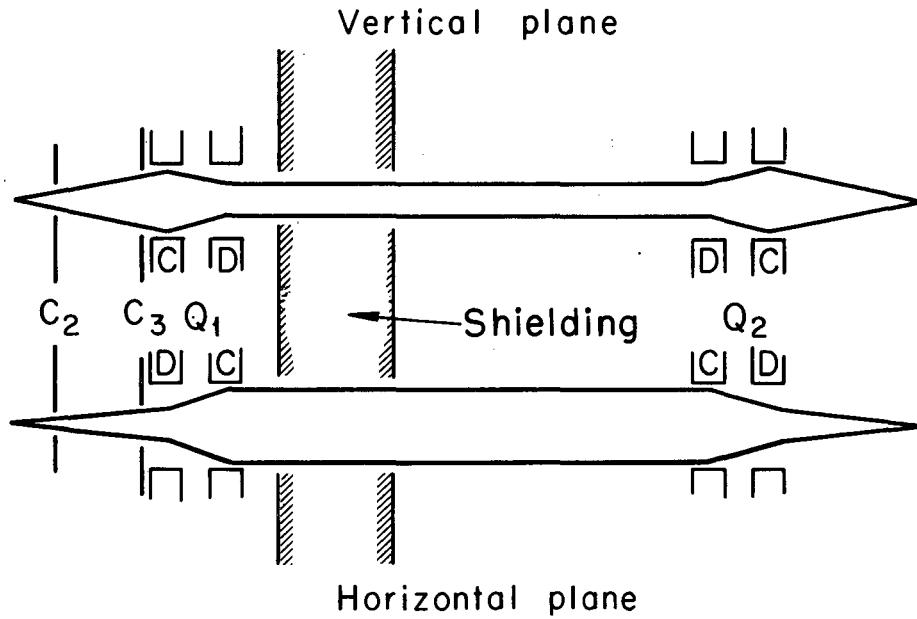
MU-34253

Fig. 4. Diagram of beam optics.
   Q = quadrupole
   C = converging quadrupole element
   D = diverging quadrupole element
   C_i = collimator

An ion chamber faced with a 0.100-in. tantalum plate containing a 1/16 × 1.5-in. slot was used to scan the beam. The chamber was moved remotely through a selsyn unit with the slot oriented vertically for the horizontal profiles and horizontally for the vertical profiles. Typical profiles are shown in Fig. 5. At the target center the beam had, in the horizontal plane, a full width at half maximum of 0.22 in. and in the vertical plane a full width at half maximum of 0.125 in.

Once the beam was optimized and the quadrupole currents set, the direction of this beam line was determined by locating, with a transit, the peak horizontal profile position at two points about 30 in. apart. The center of the scattering table was located on the transit line and the zero degree marker on the table rotated to coincide with the beam line. During the run the possible beam drift was monitored with a split ionization chamber, which could detect a beam displacement of 0.002 in.

By use of a Faraday cup and an aluminum foil wheel, an integral range curve was taken. The results are shown in Fig. 6. The tables of Williamson and Boujot[11] were used to convert the Al foil thickness to energy equivalents, and the tables of Livingston and Bethe[12] were used to correct for the loss in air. With the deuterium target at 114.7 psia and room temperature, the beam energy at the center was 40.3 ± 0.5 MeV.

To check the geometrical alignment, target T_2 was filled with hydrogen gas and the asymmetry ϵ for p-p scattering was measured. Since the value of p-p polarization at 40 MeV is close to zero, no asymmetry should have been observed. Since the measured asymmetry was < 0.002 ± 0.0005, the alignment was considered to be good enough so that any corrections due to alignment errors could be ignored.

B. Scattering Table

The scattering table, target, and counter arms are shown in Fig. 7, with a plan view of one counter setup shown in Fig. 8. The circumference of the scattering table was graduated from 0 to 360 deg in 1-deg steps. Eight counters could be operated at once, four on the left, four on the right. Two counters were on separate arms, while for the
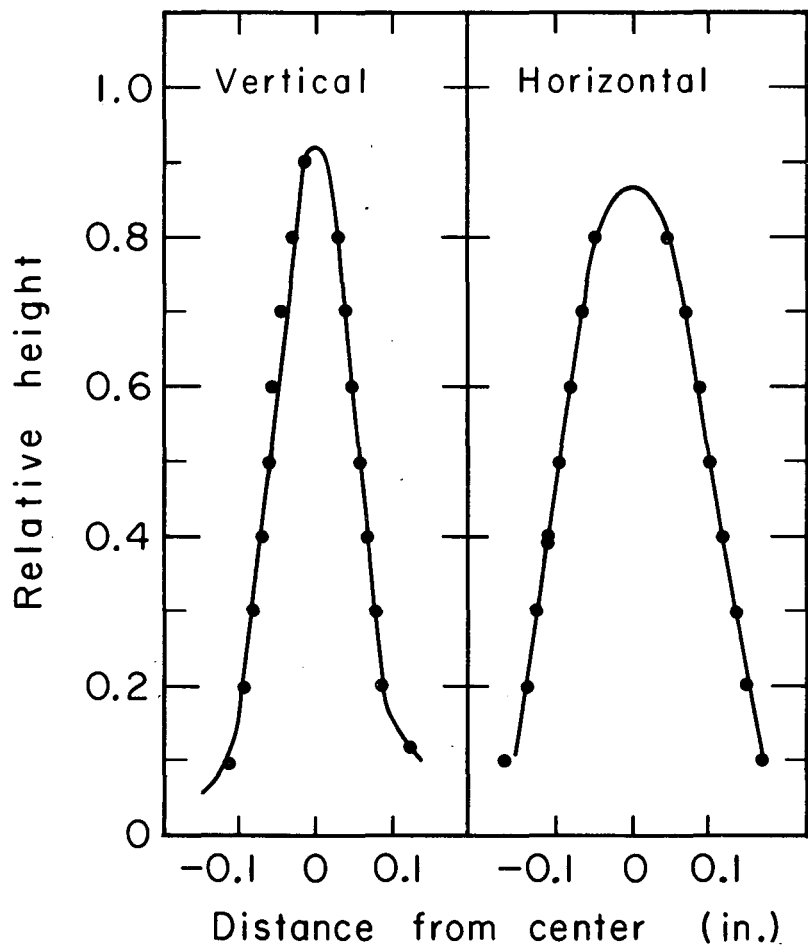
Fig. 5. Beam profiles.
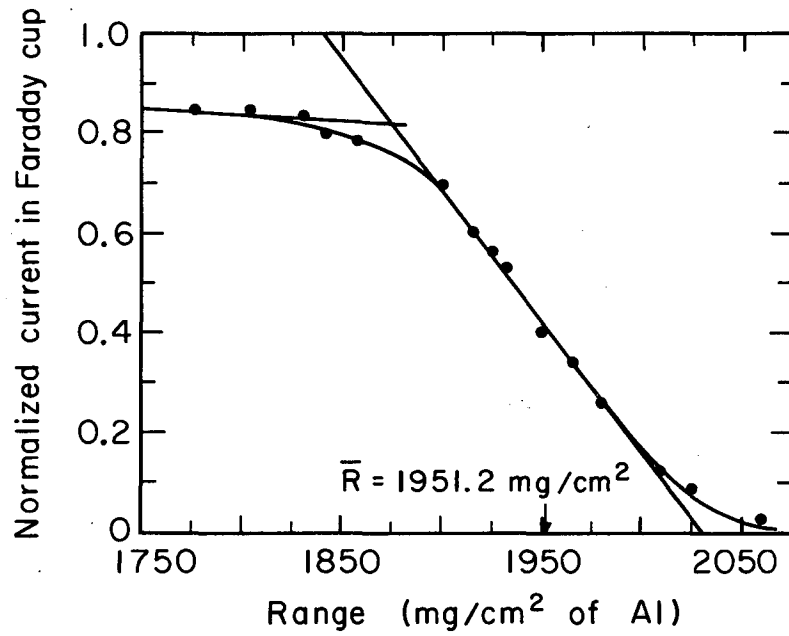
Fig. 6. Integral range curve for 40-MeV proton beam.
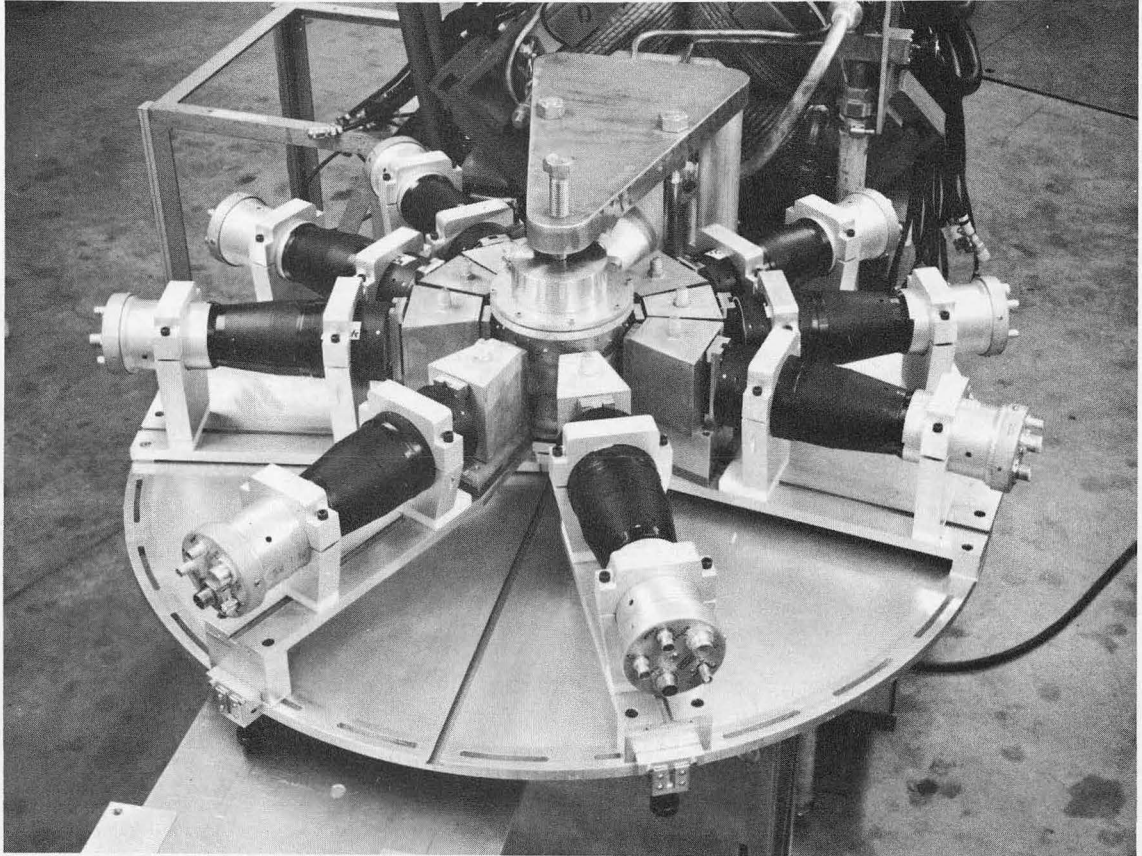
ZN-4346

Fig. 7. Scattering table and counter setup.
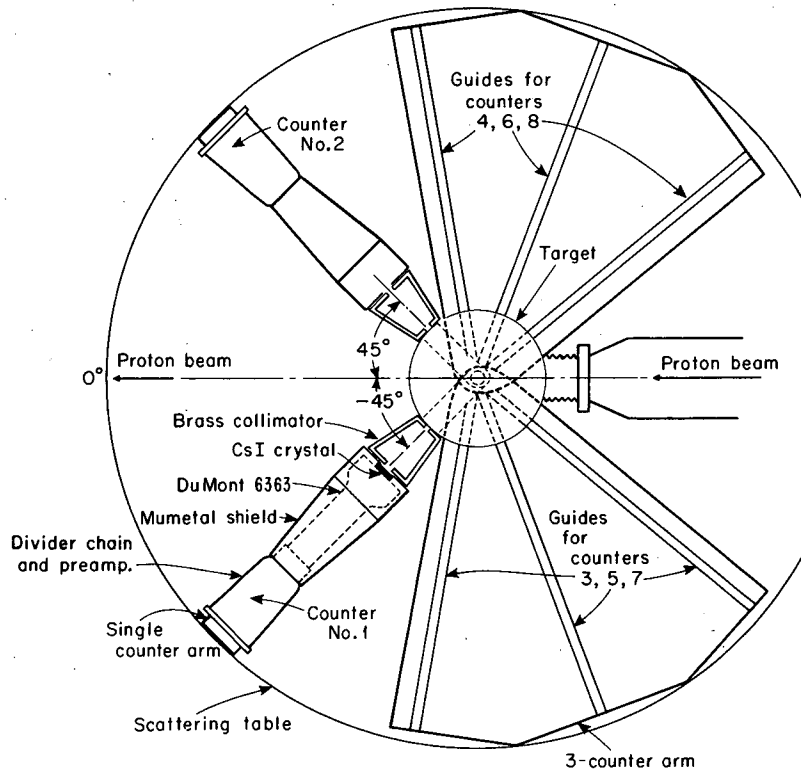
Fig. 8. Top view of scattering table and a pair of counters, showing collimators, CsI crystal orientation, and counter arms.

other six, three were on one arm, three on another. In this way, while slow rate data were being collected at three backward angles the forward counter could be swept through several angles. The trapezoidal brass houses were necessary to collimate the scattered proton beam. Each house contained two slots 3/8 in. wide and 2.5 in. high. They determined the solid angle and the angular aperture. The former was 0.01884 steradian and the latter was ± 1.5 degrees.

During the experiment the target was run at 114.7 psia and room temperature. The target windows were 0.015-in. Mylar, and the separation foil between the target and the cyclotron vacuum system was 0.005-in. Mylar. As one can see from Fig. 9, the Mylar window extended continuously most of the way around the target so that only about 30 deg in the back direction was lost.

C. Detection System--Counters

The proton detection system was a CsI crystal mounted on a Dumont 6363 phototube with a 3-in. photocathode. Initially the resolution of each system was tested by using a Cm^{244} α source, with the phototube and source mounted in an evacuated chamber. With the CsI crystal mounted directly to the face of the phototube, the α resolution was on the order of 16%, not a very satisfactory number. Using a light pulser and 1/4-in. D mercury lamp, the tube output was measured as the lamp moved over the face of the phototube and found to vary in spots by as much as a factor of 6, often being lowest in the center. A typical map over the phototube face of a normalized number, ρ, proportional to the tube output is shown in Fig. 10. If one tried to orient the CsI crystal along a line of constant ρ the resolution improved, but only by a small amount. However, by silicon greasing on a 1/2-in. polished glass pipe and aligning the crystal along a relatively constant value of ρ, the resolution was improved, by a factor of 2 to 3, to 4 to 5%. Another trouble with our batch of 6363's was that the gain drifted by as much as 20% over a 24-hr. period. This required careful selection of tubes and short experimental runs.
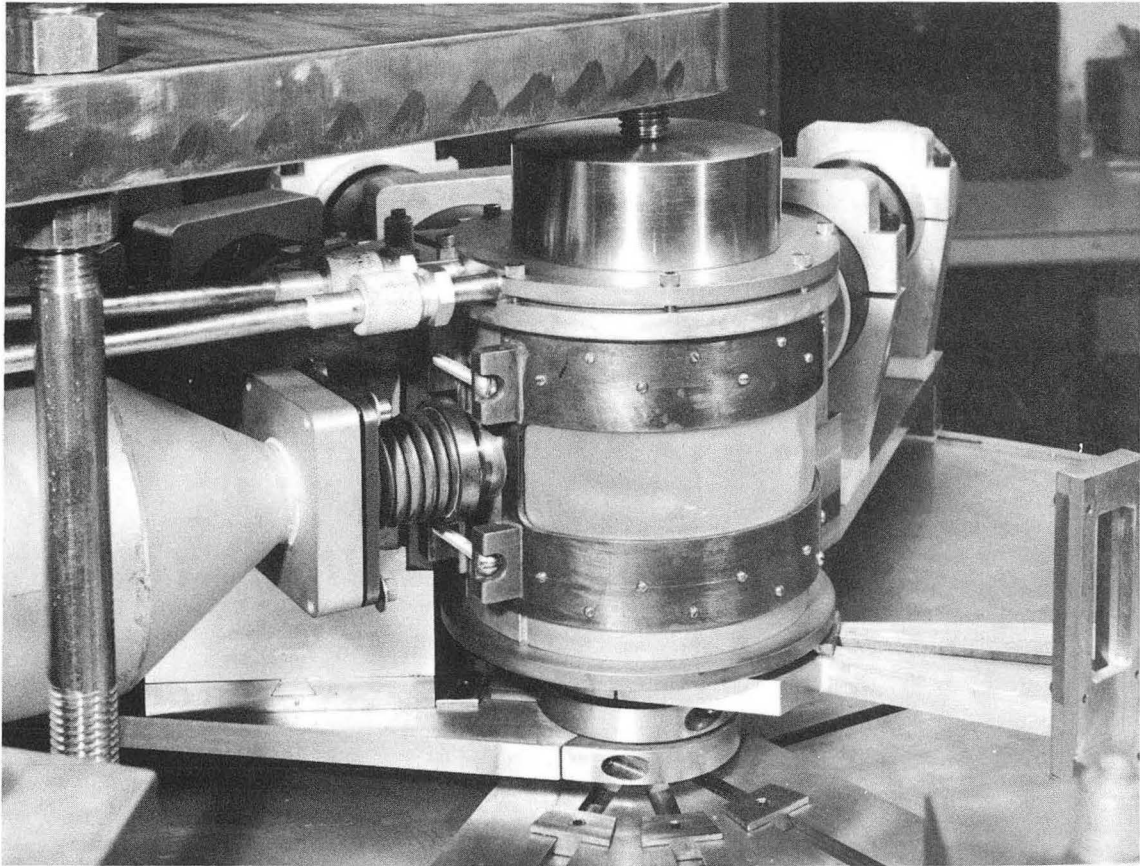
ZN-4347

Fig. 9.   Gaseous deuterium target.
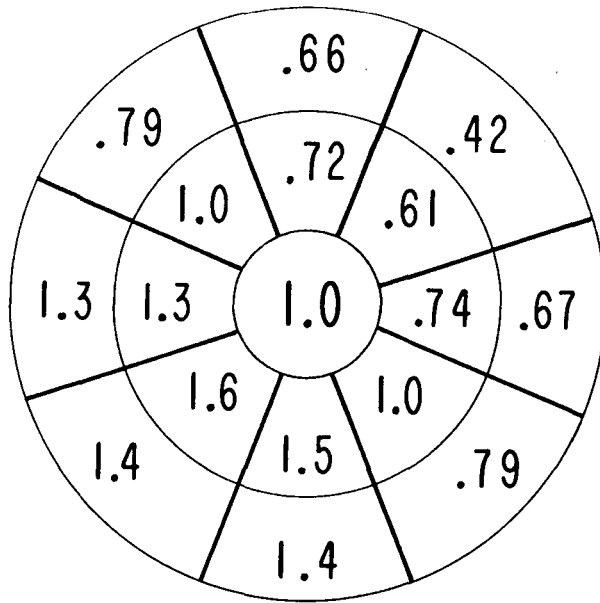
MU-34257

Fig. 10. Relative values of light output over the face of a
Dumont 6363 phototube.

The crystals were 1 in. wide by 3 in. long, and came in thicknesses of 0.400, 0.200, 0.100, 0.050, and 0.025 in. This allowed us to stop the high-energy protons, when counting in the forward directions, and minimize the background when counting in the backward directions.

The resolution was further checked by using 30-MeV protons scattered on polyethylene, and found to be on the order of 1.5% at these higher energies.

D. Detection System--Electronics

The phototube base was a standard linear 150 K resistor chain. The signal was taken off the last dynode and fed into a charge-sensitive preamplifier built into the phototube base. The eight signals were taken directly from the experimental area into the counting area and split into two groups of four. A block diagram of either group is shown in Fig. 11. The preamplifier signal first entered an amplifier-crossover unit. The amplifier section inverted the input pulse and amplified it enough to match the 8-volt input range of the pulse-height analyzer. The crossover section shaped the RC pulse before sending it onto a router-mixer unit. Here, the amplified pulses were mixed and the single output fed into the PHA. The crossover signals were sent to a router section which triggered a shaped routing pulse. In this way counter 1 was routed into channel 0-99, counter 2 into channel 100-199, counter 3 into channel 200-299, and counter 4 into channel 300-399, or counters 5, 6, 7, and 8, respectively. Each routing pulse produced a gating pulse which was set in coincidence with an on-off signal from a scaler gater unit. When two counter signals arrived simultaneously the gating pulse was suppressed. The output of the coincidence unit was fed into the delayed coincidence input of the PHA. In this way the PHA was turned off unless a single event occurred. Two PHA's were used so that eight counters could be operated simultaneously. An ion chamber, set behind T_2, was used to monitor the beam.
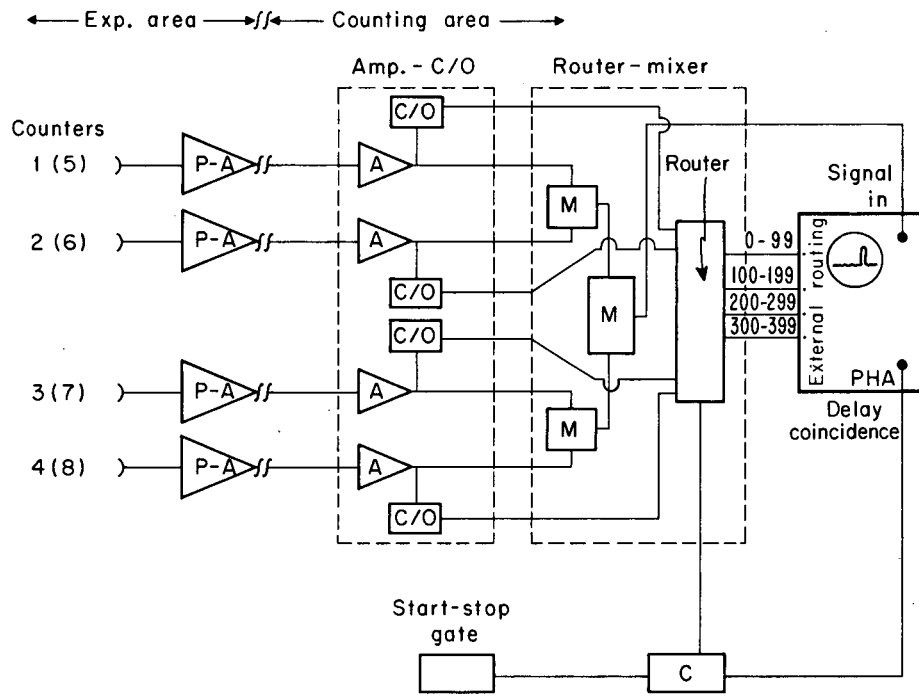
Fig. 11. Electronics block diagram.

A	= amplifier
P-A	= preamplifier
C/O	= baseline crossover
M	= mixer
PHA	= pulse-height analyzer
C	= coincident

V. DATA ANALYSIS

A. Data Reduction

Since no conjugate counter was used, the PHA display contained, along with the spectra from the elastic protons, spectra due to various background events. In order to arrive at the final polarization the background process had to be distinguished from the elastic proton events and subtracted from them. The particles from the competing processes were elastic recoil deuterons, inelastic protons which arose from the breakup of the deuteron in $p + d \rightarrow p + p + n$, target-empty events, and γ rays, which converted in the CsI crystal to give a large low-energy spectrum. Figures 12, 13, and 14 illustrate typical spectra in which one or more of the above background processes were present.

Figure 12 was typical of the spectrum at forward angles ($\theta_L \leqslant 35$ deg). The number of elastic protons was estimated by taking the counts of the high-energy side (BC) of the peak (A'BC) and doubling them, i.e., by making the low-energy side the mirror image of the high-energy side. Since the maximum energy of the inelastic proton is 2.23 MeV less than the corresponding elastic proton, or four or five PHA channels, the distortion due to inelastic events is much less on the high-energy side of the peak. The earlier work on calibrating the counters showed them to give an inherently symmetric peak. The normalized target-empty counts were then subtracted from the counts under ABC to give the number of elastic protons. Because of the relatively high energy of the protons (≈ 36 MeV) and their relatively large elastic differential cross section (≈ 100 mb/sr), the proton peak stood out well from the low-energy background and inelastic protons. For these forward angles 0.400-in. CsI crystals were used.

At backward angles ($\theta_L \geqslant 65$ deg) with the proton energy reduced ($\leqslant 20$ MeV) and the elastic cross section down by at least a factor of 25 $[\sigma(\theta) \leqslant 4$ mb/sr$]$,[4] the elastic peaks would have been indistinguishable from the inelastic background had not the crystals been made much thinner than 0.400 in. The very back counters were 0.025 in. thick, and
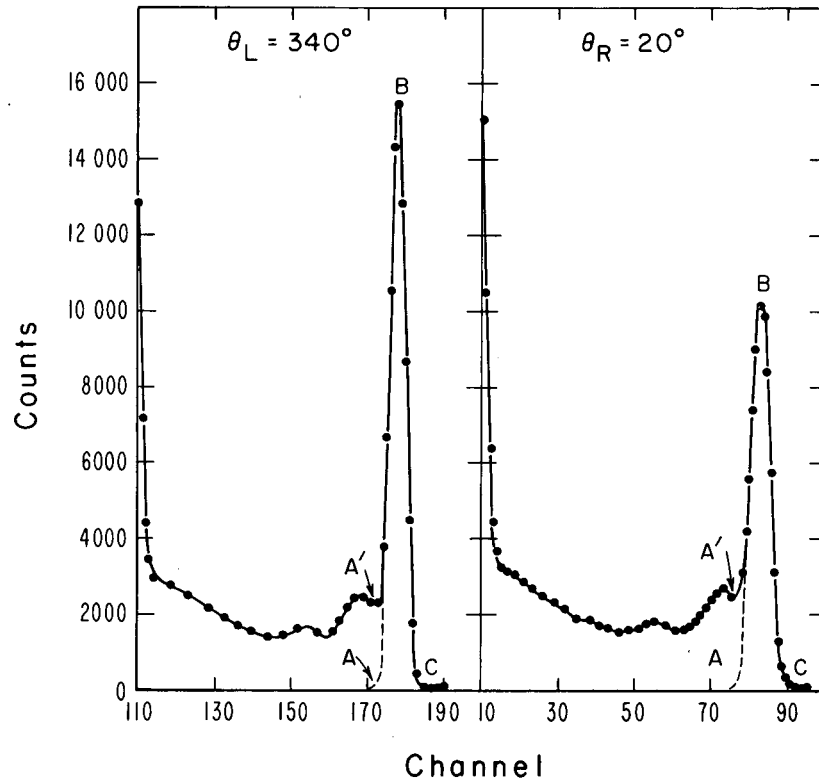
Fig. 12. Pulse-height spectra at equal left and right angles
($\theta = 20$ deg) showing the elastic proton peak.
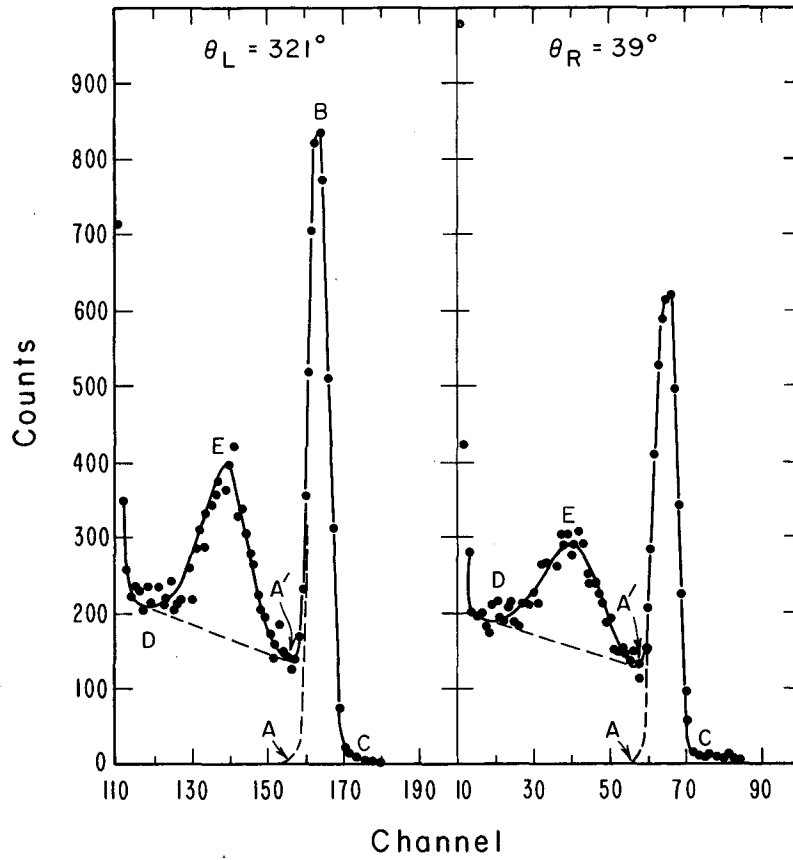
Fig. 13. Pulse-height spectra at $\theta = 39$ deg, showing the elastic proton peak and recoil deuteron peak.
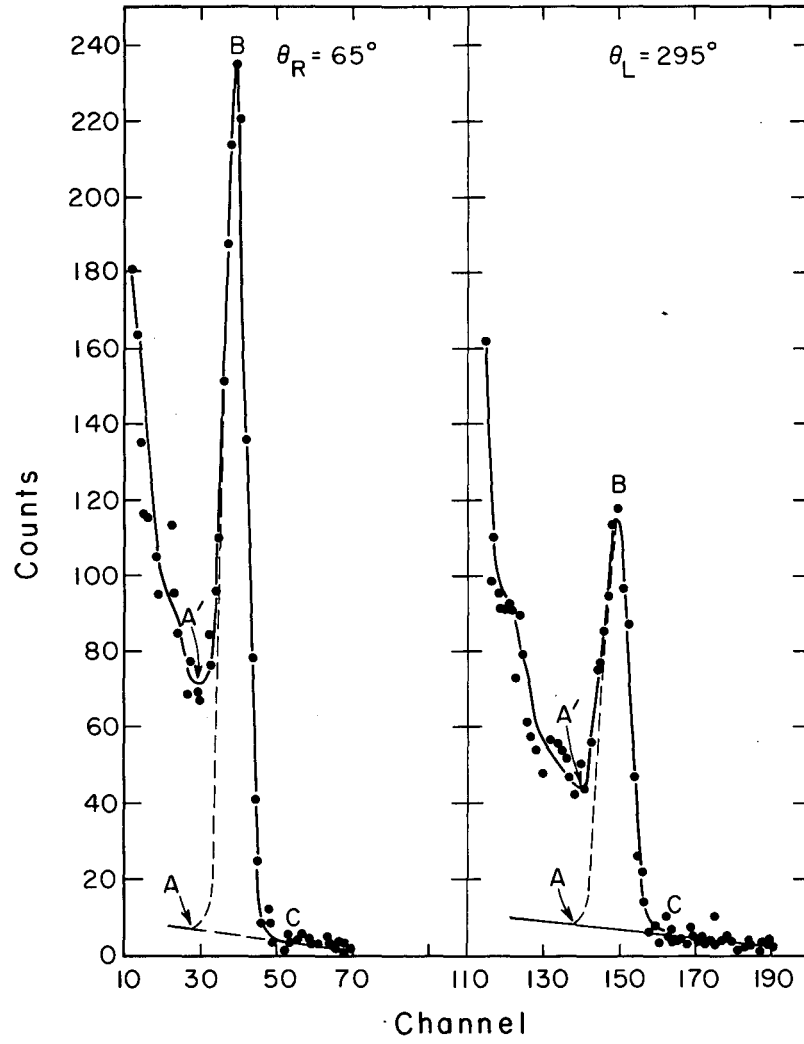
Fig. 14. Pulse-height spectra at $\theta = 65$ deg, showing the elastic proton peak.

MU-34281

counters of 0.050 and 0.100 in. were used at more forward angles. The counters were reduced in thickness in order to cut down the number of gammas converting in the CsI, but were left large enough to stop the elastic proton at the particular angle in question. A typical spectrum is shown in Fig. 14. To find the elastic proton counts the high-energy side of the peak (BC) was again doubled, but this time to the line AC, which was determined by extrapolating the high-energy tail. Subtracting the counts under AC from those under ABC gave the number of elastic protons.

At $\theta = 30$, 35, 39, and 45 deg, along with the elastic proton peak was a peak due to the recoil deuterons. This can be seen clearly in Fig. 13. The number of recoil deuterons was the number of counts under DEA' minus the number of counts under DA'. It was assumed that the recoil deuterons were sitting on the background spectra of the inelastic events. The recoil deuteron asymmetry gave the asymmetry of the associated backward-scattered proton, and provided a check on the backward-angle data. The elastic proton peak was treated in the same way as the above described forward angle case, i.e. by doubling the high-energy side of the proton peak and subtracting the target-empty background.

In this way the elastic peak counts were determined on the left (L) and right (R), and the asymmetry $\epsilon(\theta) = (L - R)/(L + R)$ was calculated. Since $\epsilon(\theta) = P_4 P(\theta)$, where P_4 is the polarization of the previously described 40-MeV proton beam, we have $P(\theta) = \epsilon(\theta)/0.819$. The results are listed and discussed in a later section.

B. Errors

In each spectrum there was a peak area (P_L, P_R) beneath which were the elastic proton counts (L, R) and the various competing background processes (B_{iL}, B_{iR}). Therefore, we have

$$L = P_L - \sum_i B_{iL}, \quad R = P_R - \sum_i B_{iR}.$$

The counting error is the statistical fluctuation in the number of counts in the peak (P_L, P_R), the statistical fluctuation in the number of counts in the target-empty background, and the statistical fluctuation in the number of counts in the inelastic background.

Since $\epsilon(\theta) = f(L, R)$, we have, assuming a Poisson distribution,[13]

$$\Delta\epsilon = \left[(\Delta\epsilon_L)^2 + (\Delta\epsilon_R)^2 \right]^{1/2} ,$$

where

$$\Delta\epsilon_L = \frac{\partial\epsilon}{\partial L}\,\Delta L, \qquad \Delta\epsilon_R = \frac{\partial\epsilon}{\partial R}\,\Delta R$$

and

$$\Delta L = \left[(\Delta P_L)^2 + \sum_i (\Delta B_{iL})^2 \right]^{1/2}$$

$$= \left[P_L + \sum_i B_{iL} \right]^{1/2} ,$$

$$\Delta R = \left[P_R + \sum_i B_{iR} \right]^{1/2} .$$

How do we get $\Sigma\, B_{iL}$? For an example, take Fig. 14. P_L was equal to the counts under $(A'BC)_L$. By symmetrizing the peak we got the curve $(ABC)_L$ and subtracted the counts under AC to get L. Since $\Sigma\, B_{iL} = P_L - L$, we have the sum over the various background counts. In this way we avoided separating out each B_i, which, because of the overlap of the inelastic processes, would have been a very tedious if not impossible job. That is, it was much easier to determine the peak counts and the elastic counts and take the summed background as their difference than to estimate each background process and then sum them.

In the case of the recoil deuteron peak the process was more straightforward, since $\sum_i B_{iL}$ is the number of counts under DA'.

Finally, we have

$$\Delta\epsilon_L = \frac{2R}{(L+R)^2} \left[P_L + \sum B_{iL} \right]^{1/2}$$

and

$$\Delta \epsilon_R = \frac{2L}{(L+R)^2} \left[P_R + \sum B_{iR} \right]^{1/2} ,$$

so that

$$\Delta \epsilon = \frac{2}{(L+R)^2} \left[R^2 (P_L + \sum_i B_{iL}) + L^2 (P_R + \sum_i B_{iR}) \right]^{1/2} .$$

At the very backward angle, $\theta_L = 114$ deg, the proton peak was so buried in the inelastic background that no unambiguous background subtraction could have been made. For this point this uncertainty in the inelastic subtraction was the greatest contribution to the error. At the other backward angles the location of the point A' was open to question. This results in an uncertainty in determining the peak counts (P_L, P_R). Since L or R was fairly uniquely determined by doubling the counts on the high-energy side of the peak, this uncertainty in P_L gave an equivalent uncertainty in ΣB_{iL}. This in turn led to an increase in $\Delta \epsilon$.

Alignment errors were insignificant, as the small value of the p-p asymmetry showed, and were ignored.

Because the counters have a dimension in the vertical direction they detect particles out of the plane which is perpendicular to the polarization direction of P_1, i.e., out of the plane of the scattering table. This would necessitate a correction to the polarization $P(\theta)$, but was small enough to be ignored.

Half way through each run, left-right detector pairs with their associated electronics were interchanged in order to minimize systematic errors and to correct for differences in detector efficiency and geometry.

Since $\epsilon(\theta) = P_1 \cdot P(\theta)$, one might expect that the error in P_1 should be included. However, since P is a normalization factor and does not contribute in a random way it was not added to $\Delta \epsilon$. The uncertainty in P_1 would just normalize the whole $P(\theta)$ curve and not change its shape.

VI. THEORY

A. Impulse Approximation

The 40-MeV p-d polarization data are shown in Table II and plotted in Fig. 15, along with the various impulse-approximation predictions by Kowalski and Feldman. Much of what follows is a summary, in a very condensed form, of their 1963 Physical Review article.

The usual method for studying high-energy (E > 100 MeV) p-d scattering has been the Chew[14] form of the impulse approximation. Here, the scattering process is taken as a simple superposition of the single scattering of the incident nucleon from each of the quasi-free target nucleons. Usually, the internal motion of the target nucleons is ignored. For small momentum transfer this seems to work very well.[15, 16]

However, with large momentum transfer several effects enter and the above picture of the scattering fails. Among these effects are the internal motion of the target nucleons, multiple scattering, binding forces, and pickup scattering. Kowalski and Feldman neglected binding forces and ignored pickup scattering in their calculations. The role played by the first two effects is discussed below.

The first problem is to define the various quantities used to distinguish the p-d system from the system made up of the incident particle and one of the target nucleons.

The p-d system is composed of three particles--the incoming proton, 1, and two target nucleons, 2 and 3. In the laboratory system we have k_1, k_2, and k_3, the momentum of particles 1, 2, and 3, respectively. We can then define

$$\vec{q} = \frac{\vec{k}_2 - \vec{k}_3}{2}$$

as the momentum of nucleon 2 with respect to the c.m. of the deuteron, and q will be used to take into account the internal motion of the target nucleons.

Table II.   Proton polarization in p-d elastic scattering at 40 MeV.
Column 3 indicates whether the proton (p) or recoil deuteron (d)
asymmetries were used to give the polarization.

θ_L	$\theta_{c.m.}$	Particle	$P(\theta)$
20	30.1	p	$+0.093 \pm 0.008$
25	37.5	p	$+0.123 \pm 0.012$
30	44.9	p	$+0.103 \pm 0.011$
35	52.1	p	$+0.128 \pm 0.012$
39	57.9	p	$+0.098 \pm 0.010$
45	66.2	p	$+0.040 \pm 0.016$
50	73.0	p	-0.012 ± 0.017
55	79.7	p	-0.095 ± 0.016
45	87.7	d	-0.250 ± 0.022
65	92.5	p	-0.294 ± 0.018
70	98.6	p	-0.281 ± 0.015
39	100.3	d	-0.327 ± 0.061
76	105.6	p	-0.331 ± 0.023
35	109.7	d	-0.374 ± 0.033
84	114.3	p	-0.392 ± 0.018
30	119.8	d	-0.385 ± 0.045
95	125.3	p	-0.310 ± 0.030
100	129.9	p	-0.366 ± 0.036
106	135.1	p	$+0.060 \pm 0.041$
114	141.5	p	$+0.490 \pm 0.20$
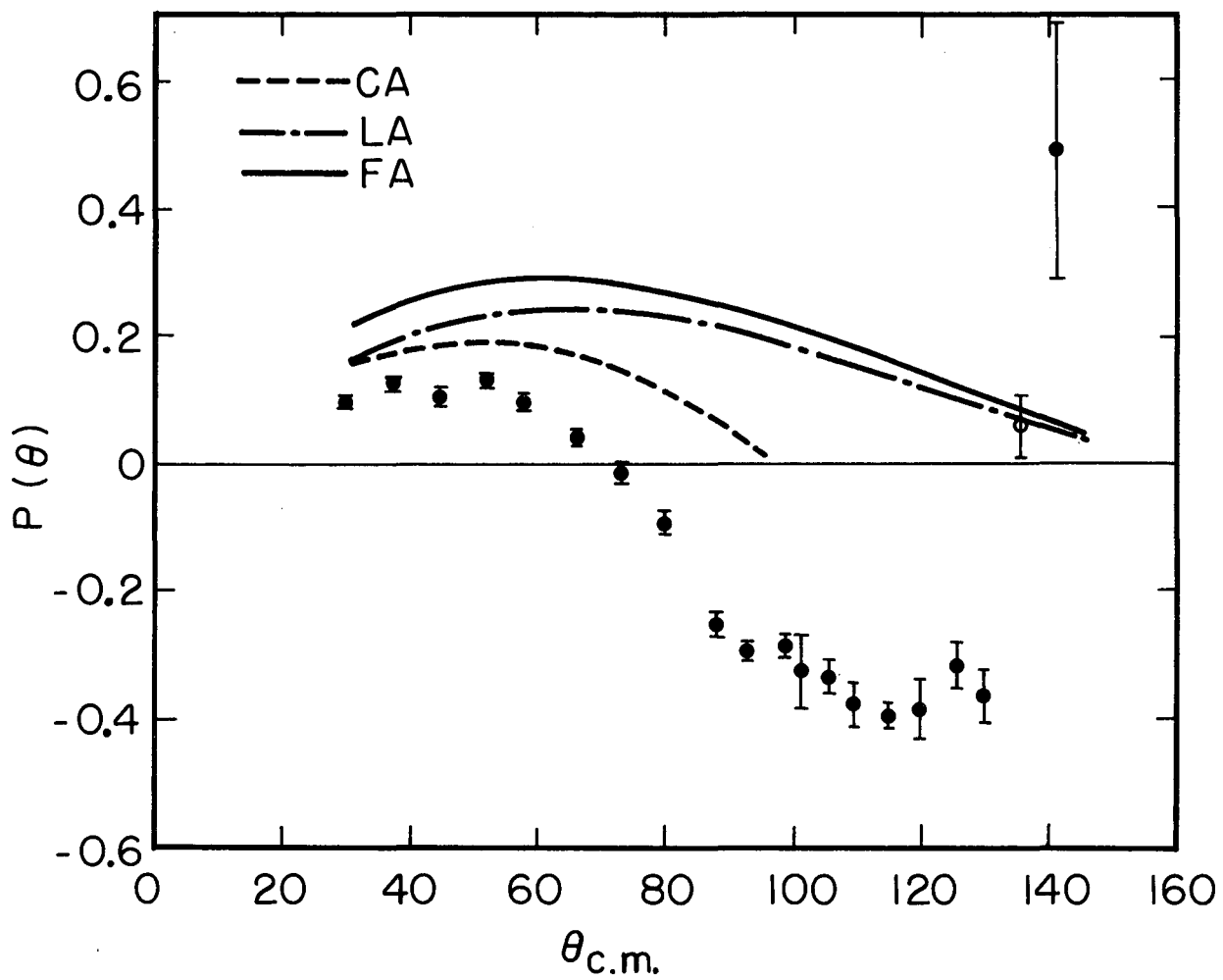
Fig. 15. Proton polarization, $P(\theta)$, in p-d elastic scattering at 40 MeV. The curves labeled CA, LA, and FA are results from impulse approximation calculations of Ref. 1.

MUB — 2813

Another quantity needed is $\vec{\eta}$, one-half the momentum transfer,

$$\vec{\eta} = \frac{\vec{k}_f - \vec{k}_i}{2}, \quad \text{where} \quad k_i = \frac{2}{3}\left[k_1 - \frac{(k_2 + k_3)}{2}\right]_i,$$

and is the momentum of the incident particles with respect to the center of mass of the deuteron, in the overall barycentric system, and $k_f = (2/3)\left\{k_1 - \left[(k_2 + k_3)/2\right]\right\}_f$ for the final particle.

Finally, we have P_i and P_f, which are, respectively, one-half the momentum of particle 1, before and after scattering, taken relative to the target nucleon off which it is scattering, which in this case is number 2. Since the impulse approximation was taken as the single scattering of the incident particle off one target nucleon, if the incident momentum of particle 1 relative to the c. m. of the deuteron is k_i then its final momentum is $\vec{k}_i + 2\vec{\eta}$, while for particle 2 if initially its momentum relative to the c. m. of the deuteron is q after colliding with 1 it will be $\vec{q} - \vec{\eta}$. Since 3 is the spectator it undergoes no change in momentum. Therefore,

$$\vec{P}_i = \frac{(\vec{k}_1 - \vec{k}_2)_i}{2} = \frac{3}{4}\vec{k}_i - \frac{\vec{q}}{2},$$

$$\vec{P}_f = \frac{(\vec{k}_1 - \vec{k}_2)_f}{2} = \frac{3}{4}\vec{k}_f - \vec{q}/2 + \vec{\eta}/2.$$

The coordinate system used to calculate $\vec{k}_i$, $\vec{q}$, and $\vec{P}_i$ is illustrated in Fig. 16. Here $k_i = 2/3\, M\dot{x}_i$, $q = M\dot{r}/2$, $P_i = M\dot{y}_i/2$, where M is the proton mass. Similarly, for the final particle, k_f, P_f, etc.

Since we are dealing with the nucleon-nucleon scattering off a deuteron target, the two-nucleon transition operator is defined as t_c with matrix elements

$$\langle \vec{P}_f, S_f | t_c | \vec{P}_i, S_i \rangle$$

where S are the total spin functions.

Lastly, we have the quantity $\phi(\vec{q})$, which is the Fourier transform of the S-state deuteron wave function and defines the momentum
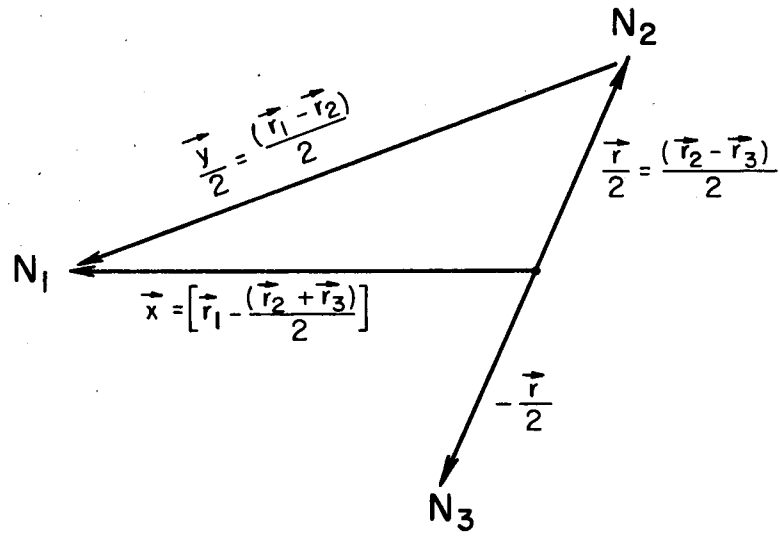
MU-34401

Fig. 16. The coordinate systems used to calculate K_i, q, and P_i (or k_f, q, and P_f).

distribution of the struck target nucleon before the collision; $\phi(\vec{q} - \vec{\eta})$ describes the momentum distribution of the struck target nucleon after collision.

The matrix element, then, that describes the scattering of an incident particle off a deuteron in the IA is[1]

$$\langle t_2(\vec{\eta}) \rangle = \int d\vec{q}\, \phi^*(\vec{q} - \vec{\eta})\, \phi(\vec{q})\, \langle \vec{P}_f, S_f | t_c | \vec{P}_i S_i \rangle \,. \qquad (1)$$

Kowalski and Feldman found that the Watson[17, 18] form of the two-body transition operator, t_c, gave the best results when compared with the Chew form.[19] Although the Watson form of t_c is an operator which encompasses multiple scattering, only the single scattering term was used.

The first approximation used to solve (1) was the Chew approximation (CA). Here q is taken as zero so that (1) separates into

$$\langle t_2(\vec{\eta}) \rangle = \langle \vec{P}_f S_f | t_c | \vec{P}_i S_f \rangle\, F_0(\vec{\eta}) \,,$$

where

$$F_0(\vec{\eta}) = \int d\vec{q}\, \phi^*(\vec{q} - \vec{\eta})\, \phi(\vec{q}) = \int d\vec{r}\, e^{i\vec{\eta}\cdot\vec{r}} |\psi(\vec{r})|^2$$

and $\psi(\vec{r})$ is the S-state deuteron wave function.

Taking q = 0 is justified only when $|\vec{\eta}|$ is small. This is because $\phi(\vec{q})$ peaks at q = 0, so that for small $\vec{\eta}$ the major contribution to (1) comes from a region about q = 0. Therefore, $\langle t_c \rangle$ is independent of q, and since the momentum transfer is small, $|P_i| = |P_f|$, so that one has on-the-energy-shell scattering.

The second approximation was the linear approximation (LA). The average value of q was defined as

$$\langle \vec{q} \rangle = \frac{\int d\vec{q}\, \phi^*(\vec{q} - \vec{\eta})\, \phi(\vec{q})\, \vec{q}}{F_0(\vec{\eta})} = \frac{1}{2}\vec{\eta} \,. \qquad (2)$$

Then $\langle t_c \rangle$ was expanded in a power series about q, retaining only the zero-order and linear terms. This gave

$$\langle t_c \rangle = \langle t_c \rangle \Big|_{\vec{q} = \langle q \rangle} + \langle \frac{t_c}{2} \rangle' \Big|_{q = \langle q \rangle} \times (\vec{q} - \langle \vec{q} \rangle) \,,$$

which, when plugged into (1), gave

$$\langle t_2(\vec{\eta}) \rangle = \langle t_c \rangle \Big|_{\vec{q}=\langle \vec{q} \rangle} F_0(\vec{\eta}) + \frac{\langle t_c \rangle'}{2} \Big|_{\vec{q}=\langle \vec{q} \rangle}$$

$$\times \left[\int d\vec{q}\, \phi^*(\vec{q} - \vec{\eta})\, \phi(\vec{q})\vec{q} - \langle \vec{q} \rangle \int dq\, \phi^*(\vec{q} - \vec{\eta})\, \phi(\vec{q}) \right].$$

But from Eq. (2) the bracketed term is zero, so that again (1) is in a separated form, and solvable.

Since $\langle \vec{q} \rangle = 1/2\, \vec{\eta}$, one can go to large momentum transfer by considering the internal motion of the target nucleons, thus extending the CA approximation. Since $|k_i| = |k_f|$, $|P_i| = |P_f|$, so that one is still on the energy shell.

The final approximation is called the off-the-energy-shell approximation (FA) where $\vec{q} = q(\vec{\eta}/\eta)$. The results are much more complicated to convey than either of the previous two cases, and are not given here. However, it does allow a solution of (1) for large momentum transfer, and--as can be seen from the equations for P_i and P_f-- now includes off-the-energy-shell scattering.

With elastic differential cross section data available at 40, 95, and 150 MeV and with polarization data available at 150 MeV, Kowalski and Feldman found the FA gave the best fit to the data, although at backward angles even the FA predictions were not very good. This is probably due to the neglect of pickup scattering which, being an exchange effect, would show up at backward angles. However, as Fig. 15 shows, the discrepancy between the experimental and calculated results increases in going to the more complete version of the calculation. At backward angles the prediction seems to break down completely, again possibly because of the neglect of pickup scattering, but the calculated curves are quite far off even at forward angles. Here, since pickup is not involved, the reason is probably the neglect of multiple scattering effect and possibly a breakdown of the IA, itself. As one goes to lower energies, multiple scattering[19]-effects become more important, and will probably have to be considered before the impulse approximation is abandoned.

B. Density Matrix Formalism of the p-d Problem

With the predictions of Kowalski and Feldman in such poor agreement with our 40-MeV polarization data, and with the inclusion of multiple scattering corrections being a very tedious job, a phase-shift analysis presented itself as a straightforward way of analyzing the data. Although much work has been done on the (1/2, 1/2) system,[5] very little has been done in formulating the (1/2, 1) problem. Two articles held out hope: one by Budianskii,[7] the other by Hsueh-tan,[8] each tackling the problem along the lines set up by Wolfenstein, that is, a density-matrix formalism. However, reflecting this age of ideological conflict, Hsueh-tan refuted the Russian work, "It may be immediately seen that the corresponding formulas in the previous work (Budianskii) are erroneous." This disagreement led us to try to reformulate the problem, to see who was correct, and then proceed with a phase-shift analysis. Unfortunately, it seems that there are errors in both papers. Therefore, in what follows the work is presented in some detail, much more so than would be necessary had a correct set of equations existed. We feel this is necessary in order to clarify our formalism of the problem. The discrepancies between the Russian and Chinese papers will be noted as they arise.

The combined spin space of two particles of spin S_1 and S_2 will have $(2S_1 + 1)(2S_2 + 1)$ basic states, χ_i, i going from 1 to $(2S_1 + 1)(2S_2 + 1)$. Any state will be a linear combination of these $(2S_1 + 1)(2S_2 + 1)$ basic states. For $S_1 = 1/2$, $S_2 = 1$ there are six basic vectors, which could be the four quartet states and the two doublet states. Any operator that describes the component system must be a $(2S_1 + 1)(2S_2 + 1)$ by $(2S_1 + 1)(2S_2 + 1)$ matrix. Any arbitrary operator can be written as a linear combination of $(2S_1 + 1)^2(2S_2 + 1)^2$ basic operators S^u, u going from 1 to $(2S_1 + 1)^2(2S_2 + 1)^2$. This complete set of basic operators satisfies

$$Tr(S^u S^v) = (2S_1 + 1)(2S_2 + 1)\,\delta_{uv} \,. \tag{1}$$

A state function χ^n, in a pure state n, can be expanded as a linear sum of the basic vectors χ_i:

$$\chi^n = \sum_{i=1}^{m} a_i^n \chi_i \qquad m = (2S_1 + 1)(2S_2 + 1) ,$$

where χ^n can be written as a column vector

$$\begin{pmatrix} a_1^n \\ \vdots \\ a_m^n \end{pmatrix} .$$

The Hermitian conjugate of χ^n is a row vector $\chi^{n+} = (a_1^{*n} \cdots a_m^{*n})$.

Therefore

$$\chi^{n+} \chi^n = Tr(\chi^n \chi^{n\dagger}) .$$

The expectation value of an operator S in the pure state n is

$$\langle S \rangle^n = \frac{\langle \chi^n | S | \chi^n \rangle}{\langle \chi^n | \chi^n \rangle} = \frac{\chi^{n\dagger} S \chi^n}{\chi^{n\dagger} \chi^n} .$$

Since $S\chi^n$ is a column vector we have

$$\langle S \rangle^n = \frac{Tr(S\chi^n \chi^{n\dagger})}{Tr(\chi^n \chi^{n\dagger})} .$$

If we have a mixed state, which is an incoherent sum of pure states, each with a statistical weight w_n, then we have

$$\langle \bar{S} \rangle = \sum_n w_n Tr(S\chi^n \chi^{n\dagger}) \Big/ \sum_n w_n Tr(\chi^n \chi^{n\dagger})$$

$$= Tr\left(S \sum_n w_n \chi^n \chi^{n\dagger} \right) \Big/ Tr\left(\sum_n w_n \chi^n \chi^{n\dagger} \right) .$$

If we define the density matrix ρ as

$$\rho = \sum_n w_n \chi^n \chi^{n\dagger} ,$$

we have as the average value of any operator S, when the measurements are made on particles in the incident beam,

$$\overline{\langle S \rangle_{inc}} = \frac{Tr(S\,\rho_{inc})}{Tr(\rho_{inc})} . \tag{2}$$

We next take the asymptotic form of the scattered wave in each pure spin state as

$$\psi_f^n(\theta, \phi) = \chi_f^n(\theta, \phi)\, e^{ikr}/r .$$

Then the amplitude of the scattered wave is given by

$$\chi_f^n(\theta, \phi) = M(\theta, \phi)\, \chi_{inc}^n .$$

This defines M, a Hermitian matrix which transforms the initial spin space into the final spin space. Therefore,

$$\rho_f = \sum_n w_n\, \chi_f^n \chi_f^{n\dagger} = \sum_n w_n\, M\chi_{inc}^n \chi_{inc}^{n\dagger} M^\dagger = M\rho_{inc}\, M^\dagger .$$

Since ρ is a matrix in our combined spin space, it can be written as

$$\rho_{inc} = \sum_u a_{inc}^u\, S^u .$$

By using (1) we have

$$a_{inc}^u = \frac{Tr(\rho_{inc}\, S^u)}{(2S_1 + 1)(2S_2 + 1)} ,$$

so that

$$\rho_{inc} = \frac{\sum_u Tr(\rho_{inc}\, S^u)\, S^u}{(2S_1 + 1)(2S_2 + 1)} ;$$

using (2), we get

$$(2S_1 + 1)(2S_2 + 1)\, \rho_{inc} = Tr(\rho_{inc}) \cdot \sum_u \overline{\langle S^u \rangle_{inc}}\, S^u .$$

Then, since $\rho = M\rho_{inc} M^\dagger$, we have

$$(2S_1 + 1)(2S_2 + 1)\, \rho_f = \mathrm{Tr}(\rho_{inc}) \cdot \sum_u MS^u M^\dagger \, \overline{\langle S^u \rangle}_{inc} \, .$$

The differential cross section is

$$I = \mathrm{Tr}(\rho_f) / T_r(\rho_{inc}) \, .$$

For an unpolarized beam the only $\langle \overline{S} \rangle$ that is nonzero is for $S^u = I_{00}$, the identity matrix. For $S_1 = 1/2$, $S_2 = 1$, we have

$$\rho_f = \mathrm{Tr}(\rho_{inc})\,(MM^\dagger)/6$$

and

$$I_0 = \frac{\mathrm{Tr}(MM^\dagger)}{6} \, .$$

For a polarized beam there are two $\langle \overline{S} \rangle$ that are nonzero. One is the previously described identity matrix, the other is for $\vec{S}^u = \vec{\sigma}$. The average value $\langle S^2 \rangle$, $\langle \vec{\sigma} \rangle_{inc} = P\hat{n}_1$ is the polarization of the incident beam. This gives

$$\rho_f = \frac{\mathrm{Tr}(\rho_{inc})}{6} \left[MM^\dagger + M\vec{\sigma} M^\dagger \cdot P_1 \hat{n}_1 \right]$$

and

$$I_f = I_0 \left[1 + \frac{\mathrm{Tr}(M\vec{\sigma} M^\dagger)}{\mathrm{Tr}(MM^\dagger)} \cdot P_1 n_1 \right] \, .$$

If we evaluate $\langle \overline{\sigma} \rangle$ for an unpolarized incident beam we have, using (2),

$$I_0 \, \overline{\langle \sigma_f \rangle} = \frac{1}{6}\,\mathrm{Tr}(M\vec{\sigma} M^\dagger) \, .$$

Since $\langle \overline{\sigma} \rangle$ is the polarization of the scattered beam, we have

$$I_0 P_2(\theta) = \frac{1}{6}\,\mathrm{Tr}(M\sigma_n M^\dagger) \, ,$$

so that

$$I_f(\theta, \phi) = I_0(\theta, \phi) \left[1 + P_1 P_2(\theta)\, \hat{n}_1 \cdot \hat{n}_2 \right] \, ,$$

which is the formula given in Sec. II, to show that the asymmetry $\epsilon(\theta) = P_1 P_2(\theta)$.

What we will do in the succeeding pages is first to expand M in terms of a set of basic matrices, and then, substituting this form of M into the expression for I_0 and P_2, evaluate the traces. This will relate I_0 and P_2 to the M matrix coefficients. Then the M matrix coefficients will be expressed in terms of the matrix elements of M, and finally these matrix elements will be related to the phase shifts. In this way I_0 and P_2 will be functions of the phase shifts.

We start with the fact that the transition matrix M must be invariant under rotation, space reflection, and time inversion. We would like to set up 36 independent matrices. For the spin-1/2 particle there will be four independent matrices in its spin space and for the spin 1 particle there will be nine independent matrices in its spin space. The composite space will be the product of these two spaces and have 36 independent matrices.

These matrices can be set up as Cartesian matrices or as irreducible tensors. For example, the spin-1/2 system has I_{00}, σ_x, σ_y, and σ_z as four independent Cartesian matrices, while I_{00}, $(\sigma_x + i\sigma_y)/\sqrt{2}$, $(\sigma_x - i\sigma_y)/\sqrt{2}$, and σ_z are the four independent matrices corresponding to a tensor of rank zero and a tensor of rank one. The same is true of the spin-1 spin space, where we have one matrix of zero rank, three of the first rank, and five of the second rank, giving a total of nine. The irreducible-tensor method was chosen since it is an easy way to generate various matrices, unique scalar products can be formed, and it is easily extended to higher spins. This approach was taken in the paper of Hsueh-tan.

Therefore, for the spin space of the spin-1/2 particle the zeroth-order and the first-order tensors are

$$\sigma_0^{\ 0} = I_{00} \text{ (the identity matrix) },$$

$$\sigma_1^{\ 1} = -\frac{1}{\sqrt{2}} (\sigma_x + i\sigma_y) ,$$

$$\sigma_1^{\ 0} = \sigma_z ,$$

$$\sigma_1^{\ -1} = \frac{1}{\sqrt{2}} (\sigma_x - i\sigma_y) .$$

In the spin space of a particle with spin 1, the zeroth-first-, and second-order tensors are

$$T_0^{\ 0} = I_{00},$$

$$T_2^{\ 2} = \frac{\sqrt{3}}{2}\left[(S_x^{\ 2} - S_y^{\ 2}) + i(S_x S_y + S_y S_x)\right],$$

$$T_1^{\ 1} = -\sqrt{\frac{3}{2}} \cdot \frac{1}{\sqrt{2}} \cdot (S_x + i\, S_y),$$

$$T_2^{\ 1} = \frac{\sqrt{3}}{2}\left[(S_z S_x + S_x S_z) + i(S_y S_z + S_z S_y)\right],$$

$$T_1^{\ 0} = \sqrt{\frac{3}{2}}\, S_z,$$

$$T_2^{\ 0} = \frac{\sqrt{3}}{\sqrt{6}}\left[-(S_x^{\ 2} + S_y^{\ 2}) + 2S_z^{\ 2}\right],$$

$$T_1^{\ -1} = \sqrt{\frac{3}{2}} \cdot \frac{1}{\sqrt{2}} \cdot (S_x - i\, S_y),$$

$$T_2^{\ -1} = \frac{\sqrt{3}}{2}\left[(S_z S_x + S_y S_x) - i(S_y S_z + S_z S_y)\right],$$

$$T_2^{\ -2} = \frac{\sqrt{3}}{2}\left[(S_x^{\ 2} - S_y^{\ 2}) - i(S_x S_y + S_y S_x)\right].$$

$T_1^{\ m}$ has been normalized by $\sqrt{3/2}$ and $T_2^{\ m}$ by $\sqrt{3}$, so that

$$\mathrm{Tr}(T_n^{\ \alpha} T_m^{\ \beta}) = 6\, \delta_{nm}\, \delta_{\alpha\beta}$$

holds true.

The $T_2^{\ m}$'s are derived from the $S_1^{\ m}$'s through

$$T_2^{\ m} = \sqrt{3} \sum_u C_{11}(2,\ m;\ u,\ m-u)\, S_1^{\ u} S_1^{\ m-u},$$

where $C_{11}(2,\ m;\ u,\ m-u)$ is the well-known Clebsch-Gordan coefficient.

The σ_x's and S_x's are 6-by-6 matrices and are derived shortly.

We now define a set of perpendicular unit vectors in the overall barycentric system:

$$\hat{n} = \hat{k}_{in} \times \hat{k}_{out},$$

$$\hat{P} = \hat{k}_{out} + \hat{k}_{in},$$

$$\hat{K} = \hat{k}_{out} - \hat{k}_{in}.$$

From each of these we form a tensor of ranks one and two. For the first-order tensors for P we have $P_1^{\ 1} = -1/\sqrt{2}\,(P_x + i\, P_y)$, $P_1^{\ 0} = P_z$,

$P_1^{-1} = 1/\sqrt{2}\,(P_x - i\,P_y)$, and similar expressions for n and K. For the second-rank tensor we have, for example,

$$(PP)_2^m = \sum_u C_{11}(2, m; u, m - u)\, P_1^u\, P_1^{m-u}\,,$$

$$(Pn)_2^m = \sum_u C_{11}(2, m; u, m - u)\, P_1^u\, n_1^{m-u}\,.$$

In Table III are shown how the various spins and momenta transform under space reflection and time inversion. We then take a variety of scalar products between the $\sigma_1^{\,m}$, $T_1^{\,m}$, and $T_2^{\,m}$ on one side and the $P_1^{\,m}$, $n_1^{\,m}$, $K_1^{\,m}$, $(PP)_2^{\,m}$, etc. on the other. These are listed in Table IV. The notation of summing over duplicated indices is used. No scalar product is taken between $\sigma_1^{\,m}$ and $T_1^{\,m}$, since

$$\sigma_1^{\,m} \cdot T_1^{\,m} = (\sigma_1^{\,m} \cdot P_1^{\,m})(T_1^{\,m} \cdot P_1^{\,m}) + (\sigma_1^{\,m} \cdot K_1^{\,m})(T_1^{\,m} \cdot K_1^{\,m}) + (\sigma_1^{\,m} \cdot n_1^{\,m})(T_1^{\,m} \cdot n_1^{\,m}),$$

and therefore $\sigma_1^{\,m} \cdot T_1^{\,m}$ is not independent of the other scalar products. Similarly we can express $T_2^{\,m} \cdot (nn)_2^{\,m}$ in terms of I_{00}, $T_2^{\,m} \cdot (PP)_2^{\,m}$, and $T_2^{\,m} \cdot (KK)_2^{\,m}$, and so it need not be included. Using the results of Table III the sign of the transformations under space reflection and time inversion are listed for each scalar product.

By taking the products between σ and T terms with the same space time signature and expanding M in terms of these, we can form a scalar which is invariant under space reflection and time inversion. Instead of having to describe M in terms of 36 independent matrices we have reduced the total to twelve. Therefore, M becomes:

$$M = I_{00}\left[A + D\,T_1^{\,m} \cdot n_1^n + G\,T_2^{\,m} \cdot (PP)_2^{\,m} + I\,T_2^{\,m} \cdot (KK)_2^{\,m}\right]$$

$$+ \sigma_1^{\,m} \cdot n_1^{\,m}\left[C + B\,T_1^{\,m} \cdot n_1^{\,m} + H\,T_2^{\,m} \cdot (PP)_2^{\,m} + J\,T_2^{\,m} \cdot (KK)_2^{\,m}\right]$$

$$+ E(\sigma_1^{\,m} \cdot P_1^{\,m})(T_1^{\,m} \cdot P_1^{\,m}) + F(\sigma_1^{\,m} \cdot K_1^{\,m})(T_1^{\,m} \cdot K_1^{\,m}) + K(\sigma_1^{\,m} \cdot P_1^{\,m})\left[T_2^{\,m} \cdot (PK)_2^{\,m}\right]$$

$$+ L(\sigma_1^{\,m} \cdot K_1^{\,m})\left[T_2^{\,m} \cdot (Kn)_2^{\,m}\right].$$

Table III.   Transformation properties of the spins and momenta under space reflection and time inversion.

Space reflection		Time inversion	
$\sigma \rightarrow \sigma$		$\sigma \rightarrow -\sigma$	
$S \rightarrow S$		$S \rightarrow -S$	
$\hat{k}_{in} \rightarrow -\hat{k}_{in}$		$\hat{k}_{in} \rightarrow -\hat{k}_{out}$	
$\hat{k}_{out} \rightarrow -\hat{k}_{out}$		$\hat{k}_{out} \rightarrow -\hat{k}_{in}$	
$\sigma_1{}^m \rightarrow \sigma_1{}^m$	$n_1{}^m \rightarrow n_1{}^m$	$\sigma_1{}^m \rightarrow -\sigma_1{}^m$	$n_1{}^m \rightarrow -n_1{}^m$
$T_1{}^m \rightarrow T_1{}^m$	$P_1{}^m \rightarrow -P_1{}^m$	$T_1{}^m \rightarrow -T_1{}^m$	$P_1{}^m \rightarrow -P_1{}^m$
$T_2{}^m \rightarrow T_2{}^m$	$K_1{}^m \rightarrow -K_1{}^m$	$T_2{}^m \rightarrow T_2{}^m$	$K_1{}^m \rightarrow K_1{}^m$
$(PP)_2{}^m \rightarrow (PP)_2{}^m$		$(PP)_2{}^m \rightarrow (PP)_2{}^m$	
$(Pn)_2{}^m \rightarrow -(Pn)_2{}^m$		$(Pn)_2{}^m \rightarrow (Pn)_2{}^m$	
$(PK)_2{}^m \rightarrow (PK)_2{}^m$		$(PK)_2{}^m \rightarrow -(PK)_2{}^m$	
$(nK)_2{}^m \rightarrow (nK)_2{}^m$		$(nK)_2{}^m \rightarrow -(nK)_2{}^m$	

Table IV. Scalar products and their signs under space reflection and time inversion.

Scalar	Space	Time	Scalar	Space	Time
I_0	+	+	I_0	+	+
$\sigma_1^m \cdot P_1^m$	-	+	$T_1^m \cdot P_1^m$	-	+
$\sigma_1^m \cdot K_1^m$	-	-	$T_1^m \cdot K_1^m$	-	-
$\sigma_1^m \cdot n_1^m$	+	+	$T_1^m \cdot n_1^m$	+	+
			$T_2^m \cdot (PP)_2^m$	+	+
			$T_2^m \cdot (KK)_2^m$	+	+
			$T_2^m \cdot (PK)_2^m$	+	-
			$T_2^m \cdot (Kn)_2^m$	-	-
			$T_2^m \cdot (Pn)_2^m$	-	-

Using

$$\sigma_1^m \cdot n_1^m = \sigma \cdot n \equiv \sigma_n .$$

$$T_1^m \cdot n_1^m = \sqrt{\frac{3}{2}} \, S \cdot n \equiv \sqrt{\frac{3}{2}} \, S_n$$

$$T_2^m \cdot (PP)_2^m = \sqrt{3} \left[(S \cdot P)^2 - \frac{2}{3} I \right] \equiv \sqrt{3} \, S_{PP}$$

$$T_2^m \cdot (Pn)_2^m = \frac{\sqrt{3}}{2} \left[(S \cdot P)(S \cdot n) + (S \cdot n)(S \cdot P) \right] \equiv \sqrt{\frac{3}{2}} \, S_{Pn}$$

and absorbing the normalization factors into the coefficients, we can simplify M to

$$M = A + DS_n + G \, S_{PP} + I \, S_{KK} + \sigma_n \left[C + BS_n + H \, S_{PP} + JS_{KK} \right]$$

$$+ E \, \sigma_P S_P + F \, \sigma_K S_K + K \sigma_P S_{Pn} + L \, \sigma_K S_{Kn} .$$

In Stapp's thesis[6] he has listed in Table F a variety of trace relations for the S_{ij} and S_i when they are 3-by-3 matrices (i and j run over P, K, and n). In Table V we have listed some of these relations for 6-by-6 matrices. With these trace relations we can evaluate the differential cross section and the polarization in terms of the M coefficients from

$$I_0 = \frac{1}{6} \, \mathrm{Tr}(MM^\dagger) \qquad I_0 P = \frac{1}{6} \, \mathrm{Tr}(M \sigma_n M^\dagger) .$$

This gives

$$I_0 = |A|^2 + \frac{2}{3} |D|^2 + \frac{2}{9} |G|^2 + \frac{2}{9} |I|^2 + |C|^2 + \frac{2}{3} |B|^2 + \frac{2}{9} |H|^2$$

$$+ \frac{2}{9} |J|^2 + \frac{2}{3} |E|^2 + \frac{2}{3} |F|^2 + \frac{2}{3} |K|^2 + \frac{2}{3} |L|^2$$

$$- \frac{2}{9} \, \mathrm{Re}(CI^* + HJ^*)$$

and

$$I_0 P = 2 \, \mathrm{Re} \left[AC^* + \frac{2}{3} DB^* + \frac{2}{9} GH^* + \frac{2}{9} IJ^* - \frac{1}{9} GJ^* - \frac{1}{9} IH^* \right] .$$

Table V. Some useful traces of the S_{ij} and S_i.

$$S_i S_j \equiv \frac{(S_i S_j + S_j S_i)}{2} - \frac{2}{3} \delta_{ij} I_{00}$$

1. $\mathrm{Tr} S_i = \mathrm{Tr}\, S_{ij} = 0$

2. $\mathrm{Tr} S_i S_j = 4\delta_{ij}$

3. $\mathrm{Tr}\, S_{ij} S_{kl} = \left[\delta_{ik}\, \delta_{jl} + \delta_{il}\, \delta_{jk} - \frac{2}{3}\, \delta_{ij}\, \delta_{kl}\right]$

It should be noted here that the above form of M differs from Budianskii's version. Part of this difference is only in appearance but part of it is real. What Budianskii failed to notice was that his values of H and K (p. 691) are equal, which reduces some of his terms to those given in Hsueh-tan's paper. This bears out the correctness of Hsueh-tan's approach to the problem. However, one real difference is the neglect by Budianskii to consider a term of the form $(S_{pp} - S_{kk})$. Unfortunately, as will be pointed out later, Hsueh-tan made several mistakes in evaluating the above M coefficients in terms of the M matrix elements, thus making his final results unusable.

Now we want to set up σ and S as 6-by-6 matrices and do so in a quartet-doublet representation. Since similar manipulations were carried out in deriving the explicit forms of σ and S, only the derivation of σ_x will be outlined.

We take as our six basis vectors the elements of the quartet and doublet spin states. For the quartet state we have

$$1 = \chi_{3/2}^{3/2} = a_{1/2}^{1/2} A_1^1 ,$$

$$2 = \chi_{3/2}^{1/2} = \sqrt{\frac{2}{3}} \, a_{1/2}^{1/2} A_1^0 + \sqrt{\frac{1}{3}} \, a_{1/2}^{-1/2} A_1^{+1} ,$$

$$3 = \chi_{3/2}^{-1/2} = \sqrt{\frac{1}{3}} \, a_{1/2}^{1/2} A_1^{-1} + \sqrt{\frac{1}{3}} \, a_{1/2}^{-1/2} A_1^0 ,$$

$$4 = \chi_{3/2}^{-3/2} = a_{3/2}^{-1/2} A_1^{-1} ,$$

and for the doublet state,

$$5 = \chi_{1/2}^{1/2} = \sqrt{\frac{1}{3}} \, a_{1/2}^{1/2} A_1^0 - \sqrt{\frac{2}{3}} \, a_{1/2}^{-1/2} A_1^1 ,$$

$$6 = \chi_{1/2}^{-1/2} = \sqrt{\frac{2}{3}} \, a_{1/2}^{1/2} A_1^{-1} - \sqrt{\frac{1}{3}} \, a_{1/2}^{-1/2} A_1^0 .$$

A linearly independent set of these basis vectors can be represented as

$$1 = \begin{pmatrix} 1 \\ 0 \\ 0 \\ 0 \\ 0 \\ 0 \end{pmatrix}, \quad 2 = \begin{pmatrix} 0 \\ 1 \\ 0 \\ 0 \\ 0 \\ 0 \end{pmatrix}, \quad 3 = \begin{pmatrix} 0 \\ 0 \\ 1 \\ 0 \\ 0 \\ 0 \end{pmatrix}, \quad 4 = \begin{pmatrix} 0 \\ 0 \\ 0 \\ 1 \\ 0 \\ 0 \end{pmatrix}, \quad 5 = \begin{pmatrix} 0 \\ 0 \\ 0 \\ 0 \\ 1 \\ 0 \end{pmatrix}, \quad 6 = \begin{pmatrix} 0 \\ 0 \\ 0 \\ 0 \\ 0 \\ 1 \end{pmatrix}.$$

We know when σ_x operates on $a_{1/2}^{\pm 1/2}$ we get $a_{1/2}^{\mp 1/2}$, i.e.,

$$\left(\begin{array}{l} \sigma_x a_{1/2}^{1/2} = a_{1/2}^{-1/2} \\ \\ \sigma_x a_{1/2}^{-1/2} = a_{1/2}^{1/2} \end{array} \right).$$

Therefore, when we operate with σ_x on $\chi_{3/2}^{3/2}$ we get

$$\sigma_x \chi_{3/2}^{3/2} = a_{1/2}^{-1/2} A_1^1 = \sqrt{\frac{1}{3}} \chi_{3/2}^{1/2} - \sqrt{\frac{2}{3}} \chi_{1/2}^{1/2},$$

which in terms of our representation of the basis vectors is

$$\sigma_x \chi_{3/2}^{3/2} = \sqrt{\frac{1}{3}} \begin{pmatrix} 0 \\ 1 \\ 0 \\ 0 \\ 0 \\ 0 \end{pmatrix} - \sqrt{\frac{2}{3}} \begin{pmatrix} 0 \\ 0 \\ 0 \\ 0 \\ 1 \\ 0 \end{pmatrix} = \begin{pmatrix} 0 \\ \sqrt{\frac{1}{3}} \\ 0 \\ 0 \\ -\sqrt{\frac{2}{3}} \\ 0 \end{pmatrix}. \tag{3}$$

Now σ_x is a 6-by-6 matrix; $\chi_{3/2}^{3/2}$ is a column vector. The product of these is a column vector which is just the first column of σ_x, given by Eq. (3). By operating with σ_x on each of the basis vectors in turn, we project out each column of σ_x. In a similar manner, by operating with σ_y and σ_z on these basis vectors we project out their columns. In an analogous way S_x, S_y, S_z are calculated. For reference the matrices are listed in Table VI.

Since we want σ_p, σ_K, and σ_n we have to consider

$$\hat{P} = \hat{k}_{in} + \hat{k}_{out} = \frac{[\cos(\theta)+1]\,\hat{z} + \sin\theta\,\sin\phi\,\hat{y} + \sin\theta\,\cos\phi\,\hat{x}}{2\cos(\theta/2)},$$

$$\hat{K} = \hat{k}_{in} - \hat{k}_{out} = \frac{[\cos(\theta)-1]\,\hat{z} - \sin\theta\,\sin\phi\,\hat{y} - \sin\theta\,\cos\phi\,\hat{x}}{2\sin(\theta/2)},$$

$$\hat{n} = \hat{k}_{in} \times \hat{k}_{out} = -\sin\phi\,x + \cos\phi\,y.$$

$$\sigma_x = \begin{pmatrix} 0 & \sqrt{\tfrac{1}{3}} & 0 & 0 & -\sqrt{\tfrac{2}{3}} & 0 \\ \sqrt{\tfrac{1}{3}} & 0 & \tfrac{2}{3} & 0 & 0 & -\tfrac{\sqrt{2}}{3} \\ 0 & \tfrac{2}{3} & 0 & \sqrt{\tfrac{1}{3}} & \tfrac{\sqrt{2}}{3} & 0 \\ 0 & 0 & \sqrt{\tfrac{1}{3}} & 0 & 0 & \sqrt{\tfrac{2}{3}} \\ -\sqrt{\tfrac{2}{3}} & 0 & \tfrac{\sqrt{2}}{3} & 0 & 0 & -\tfrac{1}{3} \\ 0 & -\tfrac{\sqrt{2}}{3} & 0 & \sqrt{\tfrac{2}{3}} & -\tfrac{1}{3} & 0 \end{pmatrix} \qquad \sigma_y = i \begin{pmatrix} 0 & -\sqrt{\tfrac{1}{3}} & 0 & 0 & \sqrt{\tfrac{2}{3}} & 0 \\ \sqrt{\tfrac{1}{3}} & 0 & -\tfrac{2}{3} & 0 & 0 & \tfrac{\sqrt{2}}{3} \\ 0 & \tfrac{2}{3} & 0 & -\sqrt{\tfrac{1}{3}} & \tfrac{\sqrt{2}}{3} & 0 \\ 0 & 0 & \sqrt{\tfrac{1}{3}} & 0 & 0 & \sqrt{\tfrac{2}{3}} \\ -\sqrt{\tfrac{2}{3}} & 0 & -\tfrac{\sqrt{2}}{3} & 0 & 0 & \tfrac{1}{3} \\ 0 & -\tfrac{\sqrt{2}}{3} & 0 & -\sqrt{\tfrac{2}{3}} & -\tfrac{1}{3} & 0 \end{pmatrix} \qquad \sigma_z = \begin{pmatrix} 1 & 0 & 0 & 0 & 0 & 0 \\ 0 & \tfrac{1}{3} & 0 & 0 & \tfrac{2\sqrt{2}}{3} & 0 \\ 0 & 0 & -\tfrac{1}{3} & 0 & 0 & \tfrac{2\sqrt{2}}{3} \\ 0 & 0 & 0 & -1 & 0 & 0 \\ 0 & \tfrac{2\sqrt{2}}{3} & 0 & 0 & -\tfrac{1}{3} & 0 \\ 0 & 0 & \tfrac{2\sqrt{2}}{3} & 0 & 0 & \tfrac{1}{3} \end{pmatrix}$$

$$S_x = \begin{pmatrix} 0 & \sqrt{\tfrac{2}{3}} & 0 & 0 & \sqrt{\tfrac{1}{3}} & 0 \\ \sqrt{\tfrac{2}{3}} & 0 & \tfrac{2\sqrt{2}}{3} & 0 & 0 & \tfrac{1}{3} \\ 0 & \tfrac{2\sqrt{2}}{3} & 0 & \sqrt{\tfrac{2}{3}} & -\tfrac{1}{3} & 0 \\ 0 & 0 & \tfrac{2}{3} & 0 & 0 & -\sqrt{\tfrac{1}{3}} \\ \sqrt{\tfrac{1}{3}} & 0 & -\tfrac{1}{3} & 0 & 0 & \tfrac{2\sqrt{2}}{3} \\ 0 & \tfrac{1}{3} & 0 & -\sqrt{\tfrac{1}{3}} & \tfrac{2\sqrt{2}}{3} & 0 \end{pmatrix} \qquad S_y = \tfrac{i}{\sqrt{2}} \begin{pmatrix} 0 & -\sqrt{\tfrac{2}{3}} & 0 & 0 & -\sqrt{\tfrac{1}{3}} & 0 \\ \sqrt{\tfrac{2}{3}} & 0 & -\tfrac{2\sqrt{2}}{3} & 0 & 0 & -\tfrac{1}{3} \\ 0 & \tfrac{2\sqrt{2}}{3} & 0 & -\sqrt{\tfrac{2}{3}} & -\tfrac{1}{3} & 0 \\ 0 & 0 & \sqrt{\tfrac{2}{3}} & 0 & 0 & -\sqrt{\tfrac{1}{3}} \\ \sqrt{\tfrac{1}{3}} & 0 & -\tfrac{1}{3} & 0 & 0 & -\tfrac{2\sqrt{2}}{3} \\ 0 & \tfrac{1}{3} & 0 & \sqrt{\tfrac{1}{3}} & \tfrac{2\sqrt{2}}{3} & 0 \end{pmatrix} \qquad S_z = \begin{pmatrix} 1 & 0 & 0 & 0 & 0 & 0 \\ 0 & \tfrac{1}{3} & 0 & 0 & -\tfrac{\sqrt{2}}{3} & 0 \\ 0 & 0 & -\tfrac{1}{3} & 0 & 0 & -\tfrac{\sqrt{2}}{3} \\ 0 & 0 & 0 & -1 & 0 & 0 \\ 0 & -\tfrac{\sqrt{2}}{3} & 0 & 0 & \tfrac{2}{3} & 0 \\ 0 & 0 & -\tfrac{\sqrt{2}}{3} & 0 & 0 & -\tfrac{2}{3} \end{pmatrix}$$

Table VI. Quartet-doublet representation of the σ and S matrices.

This gives, setting $\phi = 0$,

$$\sigma_P = [(\cos\theta + 1)\,\sigma_z + \sin\theta\,\sigma_x]\,/2\,\cos\theta/2\,,$$

$$\sigma_K = [(\cos\theta + 1)\,\sigma_z - \sin\theta\,\sigma_x]\,/2\,\sin(\theta/2)\,,$$

$$\sigma_n = \sigma_y\,,$$

with similar expressions for S_p, S_K, and S_n.

We also want a quartet-doublet representation for M. This means M will have the form

$$
M =
\begin{pmatrix}
M_{33} & M_{31} & M_{3-1} & M_{3-3} & & \\
M_{13} & M_{11} & M_{1-1} & M_{1-3} & & 0 \\
M_{-13} & M_{-11} & M_{-1-1} & M_{-1-3} & & \\
M_{-33} & M_{-31} & M_{-3-1} & M_{-3-3} & & \\
& & & & M_{11} & M_{1-1} \\
& 0 & & & M_{-11} & M_{-1-1}
\end{pmatrix}\,,
$$

where $M_{m'_s,m_s}$ represents an initial state with spin projection m_s, and a final state with spin projection m'_s. Here the ϕ dependence of M has been dropped by setting $\phi = 0$.

Following Blatt and Beidenharn,[20] we write, for the matrix elements of M,

$$
M_{m_s,m'_s} = \sum_J \sum_{\ell,\ell'} i^{\ell-\ell'}\,\pi^{1/2}(2\ell+1)^{1/2}\,C_{\ell s}(J,M;m_\ell m_s)\,C_{\ell' s}(J,M;m_{\ell'}m'_s)
$$

$$
\times\,(\delta_{\ell\ell'} - S_{s\ell',s\ell})\,Y_{\ell'}^{m_{\ell'}}(\theta,\phi)\,,
$$

where $Y_{\ell'}^{m_{\ell'}}$ are the spherical harmonics and $S_{S\ell',S\ell}^{J}$ are the S-matrix elements which determine the amplitude of probability flux of the outgoing waves from the amplitude of probability flux of the incoming waves. Also $\vec{J} = \vec{\ell} + \vec{S} = \vec{\ell'} + \vec{S}$, where ℓ,ℓ' are the angular moments of the initial and final states respectively, and S is the total spin of incident state, which is either 3/2 or 1/2.

Since $\vec{\ell} = \vec{r} \times \vec{p}$, $\vec{\ell}$ is perpendicular to the z direction and therefore $m_\ell = 0$. This gives the total spin projection M as $M = m_s = m_{\ell'} - m_s'$ which in turn gives $m_{\ell'} = m_s - m_s'$.

Using the characteristics of Clebsch-Gordan coefficients,[8]

$$C_{\ell s}(J, M; m_\ell, m_s) = (-1)^{\ell+s-J} C_{\ell s}(J, -M; -m_\ell, -m_s) ,$$

we can write

$$C_{\ell s}(J, m_s; 0, m_s) C_{\ell' s}(J, m_s; m_s - m_s', m_s') ,$$

$$= (-1)^{\ell+\ell'} C_{\ell s}(J, -m_s; 0 - m_s) C_{\ell' s}[J, -m_s, -(m_s - m_s'), -m_s'] .$$

Therefore the elements $M_{m_s, m_s'}$ and $M_{-m_s, -m_s'}$ will have the same products of Clebsch-Gordan coefficients. Since $Y_\ell^m = (-1)^m Y_\ell^{-m*}$, we will have

$$a = M_{33} = M_{-3-3}, \qquad g = M_{3-1} = M_{-31},$$

$$d = M_{11} = M_{-1-1}, \qquad b = M_{13} = -M_{-1-3},$$

$$c = M_{31} = -M_{-3-1}, \qquad k = M_{1-3} = M_{-13},$$

$$h = M_{3-3} = -M_{-33}, \qquad f = M_{1-1} = -M_{-11},$$

$$u = M_{11} = M_{-1-1},$$

$$v = M_{1-1} = -M_{-11}.$$

Furthermore, from the relation[8]

$$C_{\ell s}(J, M; m_\ell, m_s) = (-1)^{\ell+s-J} C_{\ell s}(J, M-1; m_\ell, m_s - 1) ,$$

we will have

$$C_{\ell s}(J, m_s; 0, m_s) C_{\ell' s}(J, m_s; m_s - m_s', m_s') = (-1)^{\ell+\ell'} C_{\ell s}(J, m_s-1; 0, m_s-1)$$

$$\times C_{\ell' s}(J, m_s - 1; m_s - m_s', m_s' - 1) ,$$

and thus

$$g = M_{3-1} = M_{1-3} = k .$$

Therefore we can write

$$
M = \begin{pmatrix}
a & c & g & h & & \\
b & d & f & g & & \\
g & -f & d & -b & & 0 \\
-h & g & -c & a & & \\
& & & & u & v \\
& 0 & & & -v & u
\end{pmatrix} .
$$

Now we can go back to our earlier expression for M and solve for the coefficients, using the properties of the traces. For example, the coefficients D and H would be

$$
D = Tr(MS_n)/Tr(S_n S_n) ,
$$

$$
H = Tr(M\sigma_n S_{PP})/Tr(\sigma_n S_{PP} \sigma_n S_{PP}) .
$$

Using the 6-by-6 representation for σ_n, σ_P, σ_K, $S_n S_P$, S_k, and $S_{PP} = S_P S_P - 2/3 \, I$, $S_{Pn} = (S_P S_n + S_n \cdot S_P)$, etc., and the simplified form of the M matrix, we get the M-matrix coefficients as functions of the M-matrix elements and θ. These are listed in Table VII.

The M-matrix elements are related to the phase shifts through the S-matrix elements. However, because the quartet spin is greater than $1/2$ there are mixing parameters in the M-matrix elements describing that state. Also, the Coulomb field must be included, since we are dealing with charged particles.

What we mean by mixing parameters is the following. If we have an initial state characterized by a fixed J and a total spin of $1/2$, then the values of ℓ, the angular momentum, that are possible are $\ell = J \pm 1/2$. This means, in going to a final state ℓ', that $\ell' = \ell$, $\ell + 1$, or $\ell - 1$. A mixing parameter would tell us to what extent the various ℓ' states were mixed. However, because of parity conservation we are limited to $\Delta \ell = 0, 2, 4$, etc. For a total spin of $1/2$, $\Delta \ell$ can only be 0 or 1, therefore, ℓ must equal ℓ' and there is no mixing.

For a total spin of $3/2$ this is not the case. Here we can have $\Delta \ell = 0, 1, 2, 3$ but, because of parity conservation, this is limited to $\Delta \ell = 0, 2$. Consider then the following:

Table VII. M-matrix coefficients expressed in terms of the
M-matrix elements.

$$A = \frac{1}{3} \; [a + d + u]$$

$$D = \frac{i}{2} \; [\frac{1}{\sqrt{3}}(c - b) + 2/3\,(f - v)]$$

$$G = \frac{3}{4} \; [\frac{(b + c)\sin\theta}{\sqrt{3}} + \frac{g}{\sqrt{3}}(1 - \cos\theta) + \frac{(a - d)}{6}(1 + 3\cos\theta)]$$

$$I = \frac{3}{4} \; [- \frac{(b + c)\sin\theta}{\sqrt{3}} + \frac{g}{\sqrt{3}}(1 + \cos\theta) + \frac{(a - d)}{6}(1 - 3\cos\theta)]$$

$$C = \frac{i}{3} \; [\frac{(c - b)}{3} + \frac{2}{3}f + \frac{1}{3}v]$$

$$B = \frac{1}{3}[d - u - \sqrt{3}\,g]$$

$$H = \frac{3i}{4} \; [\frac{(c - b)(1 + 3\cos\theta)}{6\sqrt{3}} + \frac{h}{2}(1 - \cos\theta) - \frac{f}{2}(\frac{7}{9} - \cos\theta) + \frac{4v}{9}]$$

$$J = \frac{3}{4}i \; [\frac{(c - b)}{6\sqrt{3}}(1 - 3\cos\theta) + \frac{h}{2}(1 + \cos\theta) - \frac{f}{2}(\frac{7}{9} + \cos\theta) + \frac{4v}{9}]$$

$$E = \frac{1}{4} \; [(a + \frac{d}{3} - \frac{4u}{3} + \frac{2g}{\sqrt{3}}) + (a - d - \frac{2g}{\sqrt{3}})\cos\theta + \frac{2(b + c)}{\sqrt{3}}\sin\theta]$$

$$F = \frac{1}{4}[(a + \frac{d}{3} - \frac{4u}{3} + \frac{2g}{\sqrt{3}}) - (a - d - \frac{2g}{\sqrt{3}})\cos\theta - \frac{2(b + c)}{\sqrt{3}}\sin\theta]$$

$$K = \frac{i}{2\sqrt{2}} \; [\frac{(c - b)}{\sqrt{6}}(1 + \cos\theta) + \frac{h}{\sqrt{2}}(1 - \cos\theta) - \frac{f}{3\sqrt{2}}(1 + 3\cos\theta) + \frac{2\sqrt{2}}{3}v]$$

$$L = \frac{i}{2\sqrt{2}} \; [\frac{(c - b)}{\sqrt{6}}(1 - \cos\theta) + \frac{h}{\sqrt{2}}(1 + \cos\theta) - \frac{f}{3\sqrt{2}}(1 - 3\cos\theta) + \frac{2\sqrt{2}}{3}v]$$

Initial state		Final state	
ℓ	$\ell' = \ell$	$\ell' = \ell + 2$	$\ell' = \ell - 2$

A $\begin{cases} J - 3/2 & J - 3/2 & J + 1/2 & J - 7/2 \\ J + 1/2 & J + 1/2 & J + 5/2 & J - 3/2 \end{cases}$

B $\begin{cases} J - 1/2 & J - 1/2 & J + 3/2 & J - 5/2 \\ J + 3/2 & J + 3/2 & J + 7/2 & J - 3/2 \end{cases}$

where the possible values of ℓ and ℓ' are given in terms of J. The states with 5/2 and 7/2 terms are impossible, since they can be reached only from a total spin of 7/2. Now, the states A mix as do the states B, but A and B do not mix with each other. That is, if we were in a J - 3/2 state to start with, we could reach only a J - 3/2 or J + 1/2 state, but not a J + 3/2 or J - 1/2 state. If we call these ℓ states

$$-3 \equiv J - 3/2 ,$$
$$1 \equiv J + 1/2 ,$$
$$-1 \equiv J - 1/2 ,$$
$$3 \equiv J + 3/2 ,$$

and define a state column vector (3, -1, 1, -3), then the S matrix must have the form

$$S^N = \begin{pmatrix} S_{3-1} & 0 \\ 0 & S_{1-3} \end{pmatrix} .$$

Because each submatrix is a symmetric, unitary 2-by-2 matrix, each will have 3 degrees of freedom, two phase shifts, and a mixing parameter. Although S is not diagonal, we can always start from some representation in which the phase shifts are the diagonal elements, and obtain S through a unitary transformation. Because of the convenience in handling the Coulomb phase shifts we choose the "nuclear-bar"[6] representation, where $S = e^{i\delta^N} U e^{i\delta^N}$. When the entire Coulomb effect can be considered to act outside the nuclear region the δ^N are the pure nuclear phase shifts.[6] U is a symmetric unitary matrix and will depend

only on the mixing parameters. In this representation we have

$$S_{3-1} = \begin{pmatrix} e^{i\delta_3^N} & 0 \\ 0 & e^{i\delta_{-1}^N} \end{pmatrix} \begin{pmatrix} \cos 2\,\epsilon^J & i\sin 2\,\epsilon^J \\ i\sin 2\,\epsilon^J & \cos 2\,\epsilon^J \end{pmatrix} \begin{pmatrix} e^{i\delta_3^N} & 0 \\ 0 & e^{i\delta_{-1}^N} \end{pmatrix},$$

$$S_{1-3} = \begin{pmatrix} e^{i\delta_1^N} & 0 \\ 0 & e^{i\delta_{-3}^N} \end{pmatrix} \begin{pmatrix} \cos 2\,\gamma^J & i\sin 2\gamma^J \\ i\sin 2\gamma^J & \cos 2\gamma^J \end{pmatrix} \begin{pmatrix} e^{i\delta_1^N} & 0 \\ 0 & e^{i\delta_{-3}^N} \end{pmatrix},$$

which on carrying out the matrix multiplication gives the expression in Fig. 17a, where the phase shifts are in the form δ_ℓ^J. The superscript N notes that these are the "nuclear" phase shifts, as distinct from those phase shifts in which the Coulomb field is included.

To include the Coulomb effect[21] we take the asymptotic form of the wave function for the Coulomb scattering of two nonidentical particles as

$$\psi = f_c\, e^{i(kr - n\ln 2kr + 2\sigma_0)}.$$

Then

$$f_c = \frac{-n}{k(1 - \cos\theta)}\, e^{-i n\ln\frac{(1-\cos\theta)}{2}}$$

where n is a parameter that determines the importance of the Coulomb effect, $n \approx (137\,\beta)^{-1}$, and

$$e^{2i\sigma_0} = \Gamma(1+in)/\Gamma(1-in).$$

The radial wave equation has regular and irregular solutions F_ℓ and G_ℓ, where

$$F_\ell(r) = \sin\left(kr - \frac{\ell\pi}{2} - n\ln 2kr + \phi_\ell\right)$$

and where

$$\phi_\ell = \sigma_\ell - \sigma_0 = \sum_{x=1}^{\ell} \arctan(n/x).$$

$$\begin{pmatrix} \cos 2\epsilon^J \exp 2i\left(\delta_3^N\right) & i\sin 2\epsilon^J \exp\left[i\left(\delta_3^N+\delta_{-1}^N\right)\right] & & \\ & & & 0 \\ i\sin 2\epsilon^J \exp\left[i\left(\delta_3^N+\delta_{-1}^N\right)\right] & \cos 2\epsilon^J \exp(2i\,\delta_{-1}) & & \\ & & \cos 2\gamma^J \exp\left(2i\,\delta_1^N\right) & i\sin 2\gamma^J \exp\left[i\left(\delta_1^N+\delta_{-3}^N\right)\right] \\ & 0 & & \\ & & i\sin 2\gamma^J \exp\left[i\left(\delta_1^N+\delta_{-3}^N\right)\right] & \cos 2\gamma^J \exp\left(2i\,\delta_{-3}^N\right) \end{pmatrix}$$

(a)

$$\begin{pmatrix} \cos 2\epsilon^J \exp\left(2i\,\delta_3^J\right)-\exp(2i\,\phi_3) & i\sin 2\epsilon^J \exp\left[i\left(\delta_3^J+\delta_{-1}^J\right)\right] & & \\ & & & 0 \\ i\sin 2\epsilon^J \exp\left[i\left(\delta_3^J+\delta_{-1}^J\right)\right] & \cos 2\epsilon^J \exp\left(2i\,\delta_{-1}^J\right)-\exp(2i\,\phi_{-1}) & & \\ & & \cos 2\gamma^J \exp\left(2i\,\delta_1^J\right)-\exp(2i\,\phi_1) & i\sin 2\gamma^J \exp\left[i\left(\delta_1^J+\delta_{-3}^J\right)\right] \\ & 0 & & \\ & & i\sin 2\gamma^J \exp\left[i\left(\delta_1^J+\delta_{-3}^J\right)\right] & \cos 2\gamma^J \exp 2i\,\delta_{-3}^J -\exp(2i\,\phi_{-3}) \end{pmatrix}$$

(b)

MUB-3941

Fig. 17.

When the nuclear force is turned on this solution is modified so that the asymptotic behavior of the radial function is now

$$U_\ell(r) = \sin\left(kr - \frac{\ell\pi}{2} - n\ln 2kr + \phi_\ell + \delta_\ell^N\right),$$

where δ_ℓ^N is the previously defined nuclear phase shift.

Now it is only in this representation that the nuclear and Coulomb phase shifts are additive. This may become more obvious if we go back to the S^N matrix. We chose the representation for S^N as $S = e^{i\delta^N} U e^{i\delta^N}$. From the above we see that the Coulomb field added a phase change, ϕ_ℓ to the basis vectors. In this representation the new S matrix will be $S = e^{i\phi} S^N e^{i\phi} = e^{i(\phi+\delta^N)} U e^{i(\phi+\delta^N)}$. Here the Coulomb and nuclear phase shifts add. However, had we chosen $S^N = U e^{i\delta^N} U$, which is a perfectly acceptable representation,[20] then $S = e^{i\phi} U e^{i\delta^N} U e^{i\phi}$ and the phase shifts would not have added in so simple a fashion.

The previously defined M matrix had a partial-wave expansion which depended on $(1 - S)$. If we introduce the R matrix as $R = S - 1$, we can write

$$R = S - 1 = S - S_c + (S_c - 1)$$
$$\equiv a + R_c .$$

If this is put back into the partial-wave expansion the Coulomb part, R_c, has an exact solution f_c. The newly defined matrix, a, is what is finally expanded in terms of partial waves. Since S_c is diagonal in ℓ we have, for the spin 3/2 state, the expression in Fig. 17b, where $\delta_\ell^J = \delta_\ell^N + \phi_\ell$.

It should be noted that for $J = 1/2$, $\epsilon^{1/2}$ and $\gamma^{1/2}$ are identically zero. For the $(-3,1)$ state, $J = 1/2$ means that ℓ' is 1 or -1. The latter is clearly impossible, therefore $\epsilon^{1/2} = 0$. For the $(3, -1)$ state ℓ' would be 0 or 2. At first glance this might seem all right, but for $\ell' = 0$ the only possible J is $J = 3/2$ and therefore $\epsilon^{1/2}$ must equal zero.

The M-matrix elements, when the Coulomb effects and the mixing parameters have been included, will be, for the quartet state,

$$M_{m_s',m_s} = \frac{(\pi)^{1/2}}{ik} \sum_{\ell,J} (2\ell+1)^{1/2} C_{\ell s}(J,m_s;0,m_s) C_{\ell s}(J,m_s;m_s-m_s',m_s')$$

$$\times a_\ell^J Y_\ell^{m_s-m_s'}(\theta,\phi)$$

$$-\frac{(\pi)^{1/2}}{ik} \sum_{\ell,J=\ell+3/2,\ell+1/2} \left(\frac{2\ell+5}{2\ell+1}\right)^{1/2} C_{\ell s}(J,m_s';m_s-m_s',m_s') C_{\ell+2,s}(J,m_s;0,m_s)$$

$$\times a^J Y_\ell^{m_s-m_s'}$$

$$-\frac{(\pi)^{1/2}}{ik} \sum_{\ell,J=\ell-1/2,\ell-3/2} \left(\frac{2\ell-3}{2\ell+1}\right)^{1/2} C_{\ell s}(J,m_s';m_s-m_s',m_s') C_{\ell-2,s}(J,m_s;0,m_s)$$

$$\times a^J Y_\ell^{m_s-m_s'}$$

$$+ f_c(\theta,\phi)\delta_{m_s,m_s'}$$

where a_ℓ^J are the diagonal elements and a^J are the off-diagonal elements. For the doublet state,

$$a(J) = \begin{pmatrix} e^{2i\delta_+^J} - e^{2i\phi_+} & 0 \\ & \\ 0 & e^{2i\delta_-^J} - e^{2i\phi_-} \end{pmatrix},$$

where δ_+^J is for the state with $\ell = J+1/2$ and δ_-^J for the state with $\ell = J-1/2$ and where $\delta_\ell^J = \delta_\ell^N + \phi_\ell$. Then the matrix elements for the doublet state will be

$$M_{m_s',m_s} = \frac{(\pi)^{1/2}}{ik} \sum_{\ell,J} (2\ell+1)^{1/2} C_{\ell s}(J,m_s;0,m_s) C_{\ell s}(J,m_s';m_s-m_s',m_s')$$

$$\times a_\ell^J Y_\ell^{m_s-m_s'}(\theta,\phi)$$

$$+ f_c(\theta,\phi)\delta_{m_s,m_s'}.$$

The M-matrix elements in terms of the phase shifts are given in Table VIII. Here we found it convenient to sum over J first and leave the elements as a sum over ℓ. Therefore we write the -3 state, a_{-3}^{J}, as $a_{\ell}^{\ell+3/2} \equiv a_{\ell}^{+3}$, etc.

Table VIII.   The M-matrix elements expressed in terms of the associated Legendre polynomials and the α-matrix elements containing the phase shifts and mixing parameters.

$$a(\theta) = f_c(\theta) + \frac{1}{2ik} \sum_{\ell=0}^{\ell_{max}} P_\ell^0(\theta) \left\{ \frac{1}{2}\left(\frac{(\ell+2)(\ell+3)}{2\ell+3}\right) a_\ell^{+3} + \frac{3}{2}\left(\frac{(\ell+1)(\ell+2)}{2\ell+3}\right) a_\ell^{+1} \right.$$

$$+ \frac{3}{2}\left(\frac{\ell(\ell-1)}{2\ell-1}\right) a_\ell^{-1} + \frac{1}{2}\left(\frac{(\ell-2)(\ell-1)}{2\ell-1}\right) a_\ell^{-3} - \frac{\sqrt{3}}{2}\left(\frac{\ell+2}{2\ell+3}\right) [(\ell+3)(\ell+1)]^{1/2} a^{+3}$$

$$\left. - \frac{\sqrt{3}}{2}\left(\frac{\ell+1}{2\ell+3}\right) [\ell(\ell+2)]^{1/2} a^{+1} - \frac{\sqrt{3}}{2}\left(\frac{\ell}{2\ell-1}\right) [(\ell-1)(\ell+1)]^{1/2} a^{-1} - \frac{\sqrt{3}}{2}\left(\frac{\ell-1}{2\ell-1}\right) [\ell(\ell-2)]^{1/2} a^{-3} \right\}$$

$$d(\theta) = f_c(\theta) + \frac{1}{2ik} \sum_{\ell=0}^{\ell_{max}} P_\ell^0(\theta) \left\{ \frac{3}{2}\left(\frac{(\ell+2)(\ell+1)}{2\ell+3}\right) a_\ell^{+3} + \frac{1}{2}\left(\frac{\ell(\ell+1)}{2\ell+3}\right) a_\ell^{+1} \right.$$

$$+ \frac{1}{2}\left(\frac{\ell(\ell+1)}{2\ell-1}\right) a_\ell^{-1} + \frac{3}{2}\left(\frac{\ell(\ell-1)}{2\ell-1}\right) a_\ell^{-3} + \frac{\sqrt{3}}{2}\left(\frac{\ell+2}{2\ell+3}\right) [(\ell+1)(\ell+3)]^{1/2} a^{+3}$$

$$\left. + \frac{\sqrt{3}}{2}\left(\frac{\ell+1}{2\ell+3}\right) [\ell(\ell+2)]^{1/2} a^{+1} + \frac{\sqrt{3}}{2}\left(\frac{\ell}{2\ell-1}\right) [(\ell+1)(\ell-1)]^{1/2} a^{-1} + \frac{\sqrt{3}}{2}\left(\frac{\ell-1}{2\ell-1}\right) [(\ell-2)\ell]^{1/2} a^{-3} \right\}$$

$$c(\theta) = \frac{1}{2ik} \sum_{\ell=1}^{\ell_{max}} P_\ell^1(\theta) \left\{ \frac{\sqrt{3}}{2}\left(\frac{\ell+2}{2\ell+3}\right) a_\ell^{+3} + \frac{\sqrt{3}}{2}\left(\frac{\ell+1}{2\ell+3}\right) a_\ell^{+1} - \frac{\sqrt{3}}{2}\left(\frac{\ell}{2\ell-1}\right) a_\ell^{-1} \right.$$

$$- \frac{\sqrt{3}}{2}\left(\frac{\ell-1}{2\ell-1}\right) a_\ell^{-3} + \frac{1}{2}\left(\frac{\ell+2}{2\ell+3}\right) \left[\frac{\ell+2}{\ell+3}\right]^{1/2} a^{+3} + \frac{3}{2}\left(\frac{\ell+1}{2\ell+3}\right) \left[\frac{\ell+2}{\ell}\right]^{1/2} a^{+1}$$

$$\left. - \frac{3}{2}\left(\frac{\ell}{2\ell-1}\right) \left[\frac{\ell-1}{\ell+1}\right]^{1/2} a^{-1} - \frac{1}{2}\left(\frac{\ell-1}{2\ell-1}\right) \left[\frac{\ell-2}{\ell}\right]^{1/2} a^{-3} \right\}$$

$$b(\theta) = - \frac{1}{2ik} \sum_{\ell=1}^{\ell_{max}} P_\ell^1 \left\{ \frac{\sqrt{3}}{2}\left(\frac{(\ell+2)(\ell+3)}{(\ell+1)(2\ell+3)}\right) a_\ell^{+3} + \frac{\sqrt{3}}{2}\left(\frac{(\ell+2)(\ell-3)}{(2\ell+3)\ell}\right) a_\ell^{+1} \right.$$

$$- \frac{\sqrt{3}}{2}\left(\frac{(\ell+4)(\ell-1)}{(2\ell-1)(\ell+1)}\right) a_\ell^{-1} - \frac{\sqrt{3}}{2}\left(\frac{(\ell-2)(\ell-1)}{(2\ell-1)\ell}\right) a_\ell^{-3} - \frac{3}{2}\left(\frac{\ell+2}{2\ell+3}\right) \left[\frac{\ell+3}{\ell+1}\right]^{1/2} a^{+3}$$

$$\left. - \frac{1}{2}\left(\frac{\ell-3}{2\ell+3}\right) \left[\frac{\ell+2}{\ell}\right]^{1/2} a^{+1} + \frac{1}{2}\left(\frac{\ell+4}{2\ell-1}\right) \left[\frac{\ell-1}{\ell+1}\right]^{1/2} a^{-1} + \frac{3}{2}\left(\frac{\ell-1}{2\ell-1}\right) \left[\frac{\ell-2}{\ell}\right]^{1/2} a^{-3} \right\}$$

Table VIII. Continued.

$$f(\theta) = \frac{1}{2ik} \sum_{\ell=1}^{\ell_{max}} P_\ell^1 \left\{ \frac{3}{2} \left(\frac{\ell+2}{2\ell+3}\right) a_\ell^{+3} - \frac{1}{2} \left(\frac{\ell+3}{2\ell+3}\right) a_\ell^{+1} + \frac{1}{2} \left(\frac{\ell-2}{2\ell-1}\right) a_\ell^{-1} - \frac{3}{2} \left(\frac{\ell-1}{2\ell-1}\right) a_\ell^{-3} \right.$$

$$+ \frac{\sqrt{3}}{2} \left(\frac{\ell+2}{2\ell+3}\right) \left[\frac{\ell+3}{\ell+1}\right]^{1/2} a^{+3} - \frac{\sqrt{3}}{2} \left(\frac{\ell+2}{2\ell+3}\right) \left[\frac{\ell+2}{\ell}\right]^{1/2} a^{+1} + \frac{\sqrt{3}}{2} \left(\frac{\ell-2}{2\ell-1}\right) \left[\frac{\ell-1}{\ell+1}\right]^{1/2} a^{-1}$$

$$\left. - \frac{\sqrt{3}}{2} \left(\frac{\ell-1}{2\ell-1}\right) \left[\frac{\ell-2}{\ell}\right]^{1/2} a^{-3} \right\}$$

$$g(\theta) = \frac{1}{2ik} \sum_{\ell=2}^{\ell_{max}} P_\ell^2 \left\{ \frac{\sqrt{3}}{2} \left(\frac{1}{2\ell+3}\right) a_\ell^{+3} - \frac{\sqrt{3}}{2} \left(\frac{1}{2\ell+3}\right) a_\ell^{+1} - \frac{\sqrt{3}}{2} \left(\frac{1}{2\ell-1}\right) a_\ell^{-1} + \frac{\sqrt{3}}{2} \left(\frac{1}{2\ell-1}\right) a_\ell^{-3} \right.$$

$$+ \frac{1}{2} \left(\frac{1}{2\ell+3}\right) \left[\frac{\ell+3}{\ell+2}\right]^{1/2} a^{+3} - \frac{\sqrt{3}}{2} \left(\frac{1}{2\ell+3}\right) \left[\frac{\ell+2}{\ell}\right]^{1/2} a^{+1} - \frac{\sqrt{3}}{2} \left(\frac{1}{2\ell-1}\right) \left[\frac{\ell-1}{\ell+1}\right]^{1/2} a^{-1}$$

$$\left. + \frac{1}{2} \left(\frac{1}{2\ell-1}\right) \left[\frac{\ell-2}{\ell}\right]^{1/2} a^{-3} \right\}$$

$$h(\theta) = \frac{1}{2ik} \sum_{\ell=3}^{\ell_{max}} P_\ell^3 \left\{ \frac{1}{2} \left(\frac{1}{(2\ell+3)(\ell+1)}\right) a_\ell^{+3} - \frac{3}{2} \left(\frac{1}{(2\ell+3)\ell}\right) a_\ell^{+1} \right.$$

$$+ \frac{3}{2} \left(\frac{1}{(2\ell-1)(\ell+1)}\right) a_\ell^{-1} - \frac{1}{2} \left(\frac{1}{(2\ell-1)\ell}\right) a_\ell^{-3} - \frac{\sqrt{3}}{2} \left(\frac{1}{2\ell+3}\right) \left[\frac{1}{(\ell+3)(\ell+1)}\right]^{1/2} a^{+3}$$

$$\left. + \frac{\sqrt{3}}{2} \left(\frac{1}{2\ell+3}\right) \left[\frac{1}{(\ell+2)\ell}\right]^{1/2} a^{+1} - \frac{\sqrt{3}}{2} \left(\frac{1}{2\ell-1}\right) \left[\frac{1}{(\ell+1)(\ell-1)}\right]^{1/2} a^{-1} + \frac{\sqrt{3}}{2} \left(\frac{1}{2\ell-1}\right) \left[\frac{1}{(\ell-2)\ell}\right]^{1/2} a^{-3} \right\}$$

$$u(\theta) = f_c(\theta) + \frac{1}{2ik} \sum_{\ell=0}^{\ell_{max}} P_\ell^0 \left\{ (\ell+1) a_\ell^+ + \ell\, a_\ell^- \right\}$$

$$v(\theta) = \frac{1}{2ik} \sum_{\ell=1}^{\ell_{max}} P_\ell^1 \left\{ a_\ell^+ - a_\ell^- \right\}$$

VII.   RESULTS OF PHASE-SHIFT ANALYSIS

Using the equations for I_0 and P on page 45, and Tables VI and VII, we can calculate the elastic differential cross section, $I_{0\ calc}(\theta_i)$, and the polarization, $P_{calc}(\theta_i)$, for a given set of phase shifts and mixing parameters. Using the variable metric minimization routine of Davidon,[22] we searched for a set of parameters which minimizes the quantity χ^2,

$$\chi^2 = \sum \left(\frac{I_{0\ calc}(\theta_i) - I_{0\ exp}(\theta_i)}{\Delta I_0} \right)^2 + \sum \left(\frac{P_{calc}(\theta_i) - P_{exp}(\theta_i)}{\Delta P} \right)^2$$

where $I_{0\ exp}(\theta_i)$ and $P_{exp}(\theta_i)$ are the experimental values of the elastic differential cross section and polarization respectively, and ΔI_0 and ΔP are the experimental errors; χ^2 is a statistical criteria of how well the calculated values fit the experimental points. If the errors ΔI_0 and ΔP obey a normal distribution and the partial waves beyond ℓ_{max} are zero, then χ^2 will have a normal distribution about $\chi_0^2 = M-N$, where M is the number of data points, 62 in our case, and N is the number of fitted parameters. The total number of parameters depends on the maximum partial wave involved and for $\ell_{max} \geqslant 1$, is $N = 8\ell_{max} + 2$.

Since χ^2 is a function of N variables it can be looked at as a surface in an $(N+1)$-dimensional space.[23] There are valleys in this surface corresponding to various local minima of χ^2. Starting with a set of parameters N_0, Davidon's routine finds that set of phase shifts which gives the local minimum of χ^2. By choosing a sufficient number of N_0's one can find the various valleys in the χ^2 surface, and from these see if any good solutions exist.

For an S- and P-wave fit there are 10 parameters with $\chi_0^2 = 52$. We tried five random sets of initial parameters N_0, and found all the minimum χ^2 to be larger than 5000. The probability that a good set of phase shifts--i. e. , a set whose calculated curves follow the mean value of the experimental points of a repeated set of experiments--will

have a χ^2 greater than 100, when calculated for a given experiment, is less than 0.003%. Therefore, a good set of phase shifts that has a χ^2 of 5000 is so extremely unlikely we have to regard that set as a poor fit to the data.

By including D waves, we have 18 parameters with $\chi_0^2 = 44$. Here 10 random sets were tried, of which five led to χ^2 between 290 and 320. This is a considerable improvement over the 10-parameter fit, but still leads to rather small probability that they represent good fits.

With the addition of F waves there are 26 parameters with $\chi_0^2 = 36$. We tried 20 random sets and found three that led to χ^2 between 135 and 149. These smaller values of χ^2 and the reduction of χ^2/χ_0^2 from the previous 10- and 18-parameter fits shows that F waves have to be included. This should not be surprising, since Johnston and Swenson[24] show that F waves were necessary to fit their 40-MeV p-p data. The large values of the mixing parameters in several of the J states indicate the presence of tensor forces.

Table IX lists the nuclear phase shifts and mixing parameters, in radians, that gave the best values of χ^2 for the 26-parameter fit. The best fit is plotted in Figs. 18 and 19. Our search has been rather limited, since only a few random sets were tried. Because of the length of time needed to fit one set we decided to give the above results and bring the paper up to date as a more complete analysis is made. This might include, beside a continued random search, looking at other energies so that only those phase shifts which are smooth functions of energy are retained. Also, the depolarization parameter, D, when measured, will give further valuable information.

Table IX. The nuclear phase shifts, $^{2S+1}X_{2J}$, and mixing parameters, $\epsilon(2J)$ and $\gamma(2J)$, in radians. The brackets following ϵ and γ contain the particular angular momentum states that are coupled. The error represents the amount that when added to the parameters, changes χ^2 by 1%. $\chi_0^2 = 36$.

Type		I $\chi^2 = 135.1$	II $\chi^2 = 145.7$	III $\chi^2 = 148.6$
$^4S_3$		0.15054 $\pm$0.0060	0.53942 $\pm$0.0043	0.15678 $\pm$0.0070
$^4P_5$		0.16213 $\pm$0.0032	0.60370 $\pm$0.0030	-0.043769 $\pm$0.0031
$^4P_3$		-0.22093 $\pm$0.0088	0.50596 $\pm$0.0041	0.33973 $\pm$0.0085
$^4P_1$		0.74220 $\pm$0.0089	-0.011161 $\pm$0.0022	-0.014755 $\pm$0.0015
$^4D_7$		0.26501 $\pm$0.0019	0.063043 $\pm$0.0038	-0.033233 $\pm$0.0022
$^4D_5$		0.13339 $\pm$0.0080	0.28907 $\pm$0.0087	0.00074131 $\pm$0.0004
$^4D_3$		0.14344 $\pm$0.0143	0.20882 $\pm$0.0062	-0.23458 $\pm$0.0010
$^4D_1$		0.21261 $\pm$0.0064	-0.27771 $\pm$0.0056	0.12358 $\pm$0.0056
$^4F_9$		-0.069461 $\pm$0.0028	0.055192 $\pm$0.0033	0.072745 $\pm$0.0043
$^4F_7$		-0.023055 $\pm$0.0037	1.6124 $\pm$0.0016	0.16130 $\pm$0.0073
$^4F_5$		0.10461 $\pm$0.0073	0.19498 $\pm$0.0039	0.065418 $\pm$0.0046
$^4F_3$		-0.37122 $\pm$0.0037	0.018139 $\pm$0.00218	0.12588 $\pm$0.0050
$\epsilon(3)$	[S, D]	0.43266 $\pm$0.0030	-0.036771 $\pm$0.0037	-0.51123 $\pm$0.0051
$\epsilon(5)$	[P, F]	0.076970 $\pm$0.0025	0.049191 $\pm$0.0034	-0.097443 $\pm$0.0029
$\epsilon(7)$	[D, G]	0.036107 $\pm$0.0054	0.15583 $\pm$0.0047	0.059628 $\pm$0.0042
$\epsilon(9)$	[F, H]	-0.022572 $\pm$0.0023	-0.12011 $\pm$0.0042	0.29921 $\pm$0.0045
$\gamma(3)$	[P, F]	0.29136 $\pm$0.0064	-0.14440 $\pm$0.0065	0.081863 $\pm$0.0057
$\gamma(5)$	[D, G]	0.10586 $\pm$0.0063	0.70083 $\pm$0.0053	-0.082578 $\pm$0.0058
$\gamma(7)$	[F, H]	-0.41340 $\pm$0.0049	1.2303 $\pm$0.0061	+0.064639 $\pm$0.0052
$^2S_1$		0.057110 $\pm$0.0086	0.16178 $\pm$0.0097	-0.012506 $\pm$0.0018
$^2P_3$		0.30103 $\pm$0.0066	0.084603 $\pm$0.0047	0.056637 $\pm$0.0056
$^2P_1$		-0.25147 $\pm$0.0101	-0.0093561 $\pm$0.0023	0.55511 $\pm$0.0056
$^2D_5$		0.34293 $\pm$0.0034	-0.06398 $\pm$0.0042	0.052231 $\pm$0.0040
$^2D_3$		0.00247 $\pm$0.0006	-0.067405 $\pm$0.0047	0.64727 $\pm$0.0051
$^2F_7$		0.33387 $\pm$0.0040	0.13039 $\pm$0.0052	0.10152 $\pm$0.0041
$^2F_5$		0.15623 $\pm$0.0055	-0.10837 $\pm$0.0065	0.59465 $\pm$0.0060
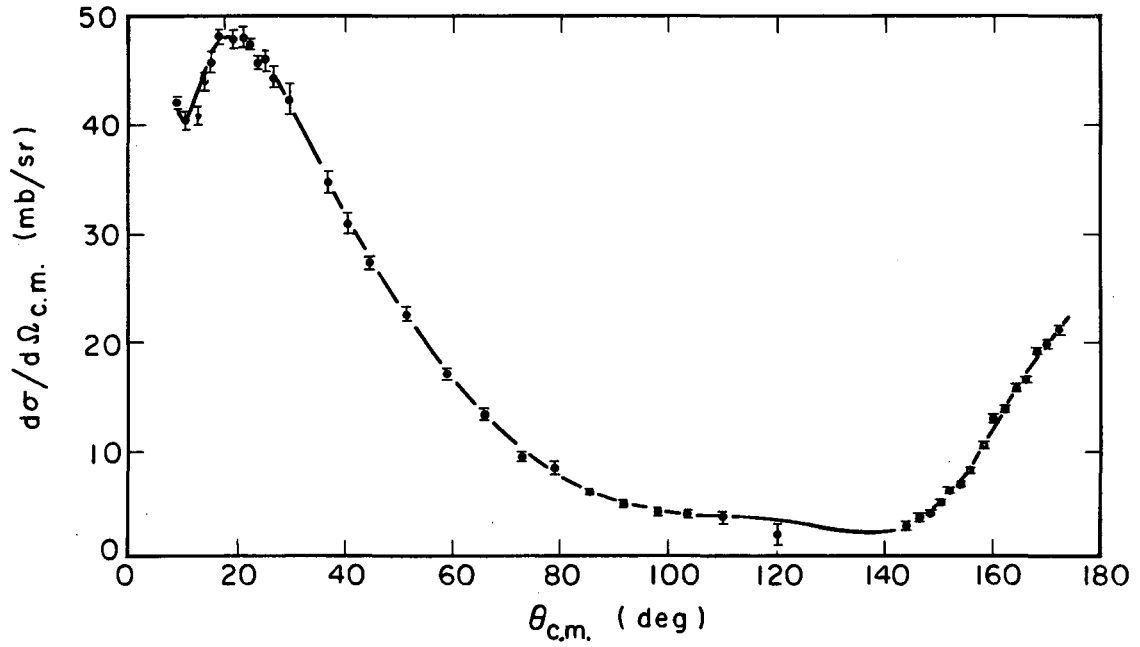
Fig. 18. The 40-MeV p-d elastic differential cross-section data from Williams. The curve is calculated from the phase shifts of Solution I.
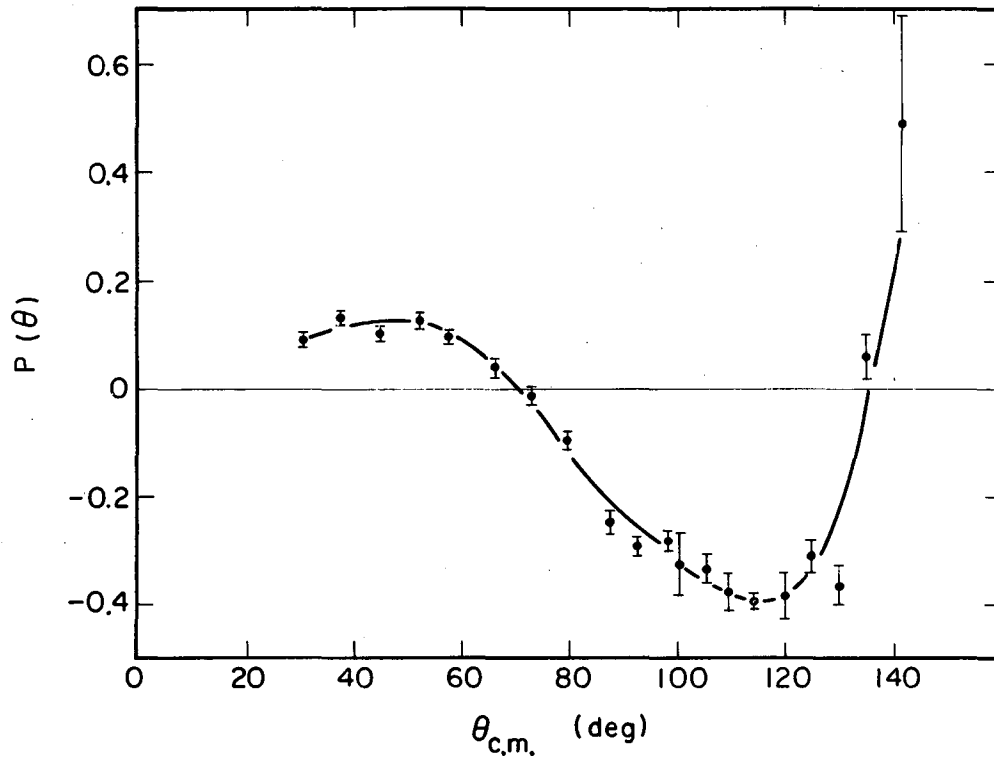
MU-34565

Fig. 19. The 40-MeV p-d polarization data from this experiment, and the curve calculated from the phase shifts of Solution I.

ACKNOWLEDGMENTS

FOOTNOTES AND REFERENCES

* This work was supported by the U. S. Atomic Energy Commission.

1. K. L. Kowalski and D. Feldman, Phys. Rev. 130, 276 (1963).

2. At 46 MeV a p-p polarization of 0.012 ± 0.013 has been reported by J. N. Palmieri, A. M. Cormack, N. F. Ramsey, and Richard Wilson, Ann. Phys. 5, 299 (1958).

3. C. F. Hwang, G. Clausnitzer, D. H. Norby, S. Suwa, and J. H. Wilharis, Phys. Rev. 131, 2602 (1963).

4. John H. Williams and Morton K. Brussel, Phys. Rev. 110, 136 (1958).

5. L. Wolfenstein and J. Ashkin, Phys. Rev. 85, 947 (1952); L. Wolfenstein, Ann. Rev. Nucl. Sci. 6, 43 (1956).

6. Henry Stapp, The Theory and Interpretation of Polarization Phenomena in Nuclear Scattering (Thesis), Lawrence Radiation Laboratory Report UCRL-3098; Phys. Rev. 103, 425 (1956).

7. G. M. Budianski, Soviet Phys. -JETP 6, 684 (1958).

8. S. Hsueh-tan, Wu Li Hsueh Pao (Acta Phys. Sinica) 16, 324 (1960).

9. L. Rosen and J. E. Brolley, Jr., Phys. Rev. 107, 1454 (1957); R. I. Brown, W. Haeberli, and J. X. Saladin, Nucl. Phys. 47, 212 (1963).

10. R. F. Burton, H. E. Conzett, H. S. Goldberg, W. L. Pope, and S. Yamabe (to be published).

11. C. Williamson and J. P. Boujot, Tables of Range and Rate of Energy Loss of Charged Particles of Energy 0.5 to 150 MeV, Report CEA-2189, Center of Nuclear Studies, Saclay.

12. M. Stanley Livingston and H. A. Bethe, Rev. Mod. Phys. 9, 245 (1937).

13. W. Edwards Deming, Statistical Adjustment of Data (John Wiley & Sons, Inc., New York, 1948).

14. Geoffrey F. Chew, Phys. Rev. 84, 1057 (1951).

15. Proceedings of the Conference on Nuclear Forces and the Few Nucleon Problem, London, 1959 (Pergamon Press, London, 1960), Vol. I.

16.   J. Sawicki and S. Watanabe, Nucl. Phys. 10, 151 (1959).

17.   Kenneth M. Watson, Phys. Rev. 89, 575 (1953).

18.   Kenneth M. Watson, Phys. Rev. 105, 1388 (1957).

19.   Geoffrey F. Chew and Gian Carlo Wick, Phys. Rev. 85, 636 (1952).

20.   John M. Blatt and L. C. Biedenharn, Rev. Mod. Phys. 24, 258 (1952).

21.   I. David Jackson and John M. Blatt, Rev. Mod. Phys. 22, 72 (1950).

22.   William C. Davidon, Variable Metric Method for Minimization, Argonne National Laboratory Report ANL-5990, 1959.

23.   M. H. Mac Gregor, M. J. Moravcsik, and H. P. Stapp, Ann. Rev. Nucl. Sci. 10, 291 (1960).

24.   L. H. Johnston and D. A. Swenson, Phys. Rev. 111, 212 (1958).